

Compound CID 9998128 Is a Potential Multitarget Drug for Alzheimer's Disease

Nguyen Quoc Thai,^{†,‡,§,◆} Zuzana Bednarikova,^{||,◆} Miroslav Gancar,^{||} Huynh Quang Linh,[§] Chin-Kun Hu,^{*,†,‡,¶,▼} Mai Suan Li,^{*,○,●} and Zuzana Gazova^{*||,●}

[†]Institute for Computational Sciences and Technology, SBI building, Quang Trung Software City, Tan Chanh Hiep Ward, District 12, Ho Chi Minh City, Vietnam

[‡]Dong Thap University, 783 Pham Huu Lau Street, Ward 6, Cao Lanh City, Dong Thap, Vietnam

[§]Biomedical Engineering Department, University of Technology -VNU HCM, 268 Ly Thuong Kiet Str., Distr. 10, Ho Chi Minh City, Vietnam

^{||}Department of Biophysics, Institute of Experimental Physics, Slovak Academy of Sciences, Watsonova 47, Kosice 040 01, Slovakia

[¶]Institute of Physics, Academia Sinica, Nankang, Taipei 11529, Taiwan

^{*}Physics Division, National Center for Theretical Sciences, Hsinchu 30013, Taiwan

[○]Department of Physics, National Dong Hwa University, Hualien 97401, Taiwan

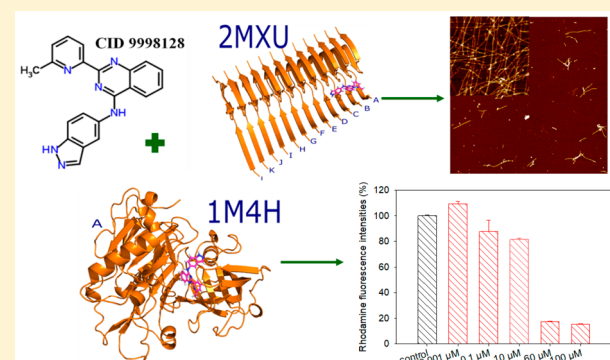
[▼]Department of Systems Science, University of Schanghai for Science and Technology, Shanghai 200093, China

[●]Institute of Physics, Polish Academy of Sciences, Al. Lotnikow 32/46, 02-668 Warsaw, Poland

Supporting Information

ABSTRACT: We have probed small molecule compound CID 9998128 as a potential multitarget drug for the Alzheimer's disease (AD) using *in silico* and *in vitro* experiments. By all-atom simulation and molecular mechanics Poisson–Boltzmann surface area (MM-PBSA) method, we have demonstrated that this compound strongly binds to both amyloid β 42 ($A\beta_{42}$) fibrils and β -secretase, and the van der Waals interaction dominates over the electrostatic interaction in binding affinity. A detailed analysis at the atomic level revealed that indazole in CID 9998128 structure made a major contribution to instability of all studied complexes. *In vitro* experiments have shown that CID 9998128 inhibits the $A\beta_{42}$ amyloid fibrillization and is capable to clear $A\beta_{42}$ fibrils. Moreover, the compound dose-dependently decreases β -site amyloid precursor protein cleaving enzyme (BACE-1) activity with EC₅₀ value in micromolar range. Thus, our study has revealed that CID 9998128 is a good candidate for AD treatment through preventing production of $A\beta$ peptides and degrading their aggregates. For drug design, we predict that the chemical structure of potent AD multitarget inhibitors should not contain indazole.

KEYWORDS: Alzheimer's disease, multitarget drug, CID 9998128, amyloid, β -secretase, protein aggregation, indazole



INTRODUCTION

Alzheimer's disease (AD) is an irreversible neurodegenerative disorder that slowly destroys memory and cognitive skills. It is the most common cause of dementia among elders, and there is currently no treatment to halt the neurodegenerative process. AD is a very complex and multifactorial disease characterized by accumulation of amyloid plaques and neurofibrillary tangles accompanied by loss of cholinergic function important for cognition and homeostasis dysregulation.¹

Due to the complex nature of AD, pathological development and molecular mechanisms of disease have not been fully explored yet. However, it is widely believed that one of the early, often initiating factors in the pathology of AD is

imbalance between production and clearance of $A\beta$ peptides in brain.² The $A\beta$ peptides are produced by proteolytic cleavage of the amyloid precursor protein (APP) by β -secretase and γ -secretase.³ Imprecise cleavage by γ -secretase is a reason behind varying length of $A\beta$ peptides containing 38–42 amino acids.⁴

The β -secretase, known as β -site amyloid precursor protein cleaving enzyme 1 (BACE1), is considered a key therapeutic target for lowering $A\beta$ concentrations in brain and clinical development of β -secretase inhibitors is being intensely

Received: February 27, 2018

Accepted: May 18, 2018

Published: May 18, 2018

pursued.⁵ Under physiological conditions, continuously produced A β peptides are efficiently cleared from brain by several pathways including proteolytic degradation, lysosomal degradation in brain parenchyma cells, or cerebrovascular system-mediated clearance.

Under pathological conditions, A β peptides accumulate within brain and form amyloid aggregates. The aggregation process starts with conformational transformation of soluble A β monomers to fibrillar structures through several structurally different aggregates such as nuclei, oligomers, and protofibrils. This dynamic process follows a nucleation–polymerization kinetic model characterized by three phases. In lag phase, soluble monomers are transformed to nuclei from which transient polymorphic soluble oligomers emerge with various cytotoxicity.⁶ After nuclei are formed, the aggregation process rapidly continues leading to conversion of oligomers into insoluble amyloid fibrils, which are the main components of amyloid plaques. Two dominant variants of A β peptide were found in amyloid plaques in brain, namely, A β_{40} and A β_{42} . Plaques also contain several truncated forms of A β peptides, such as A β_{5-42} , A β_{1-26} , and A β_{1-30} .⁷ Moreover, it has been shown that aggregation of A β_{42} could be further described by secondary nucleation process where formation of fibrils is accelerated by elongation of aggregates through the binding of monomers to the surface of formed fibrils.⁸ Therefore, the most promising approaches to handle AD based on amyloid hypothesis are focused on development of compounds capable of inhibiting or reversing amyloid aggregation of A β peptides and modulating the activity of β -secretase and γ -secretase.⁹ Moreover, researchers are further focused on improvement of A β clearance through exploring the role of apolipoprotein E (ApoE) and related receptors in AD development.

Diverse strategies have been proposed to identify potential therapeutic agents for treatment of AD. Currently studied therapeutic agents could be divided into different classes depending on their chemical and physical properties, as well as their therapeutic targets. Several small molecules,^{10,11} metal chelators,¹² short peptides,¹³ and other compounds have shown unreasonable ability to affect development of AD, though they generally affect just one specific target. It was generally accepted that small molecules designed as potential drug candidates have three modes for inhibitory action: (i) binding to the fibrils and reducing the toxicity by limiting the fibril fragmentation (BAF31);¹⁴ (ii) speeding up fibril formation and reducing the lifetime of toxic oligomers (orcein-related polyphenol);⁷ (iii) interaction with oligomers preventing fibrillization, which results in off-pathway and nontoxic species (epigallocatechin gallate (EGCG), carnosine, quinones, and quinone derivatives).^{15–17} Wang et al. have reported that EGCG is able to redirect the A β aggregation pathway generating off-pathway nontoxic oligomers, which are incapable of amyloid fibrillogenesis, and remodel mature A β fibrils into nontoxic oligomers as it binds to residues 1–16 through hydrogen bonding and residues 17–42 through hydrophobic interactions.¹⁵ Several nonpolyphenol molecules were shown to inhibit A β fibrillogenesis through binding to oligomers. Quinones and quinone derivatives were able to inhibit A β_{42} fibril formation by A β_{42} and completely recover the phenotype in a transgenic AD *Drosophila* model.¹⁷ However, it is not always clear at which stages of the aggregation pathway the small molecules are effective.¹⁸ Moreover, they can only bind weakly to the random coil A β monomers (micromolar at best) and possess higher affinity for structured aggregates (protofibrils and fibrils), but

the interactions are not tight and specific.¹⁹ Therefore, several studies argued that a better approach, if dealing with such a complex disease, is a novel multitarget-directed ligand (MTDL) strategy based on the assumption that a single compound is able to hit multiple targets.^{20,21} The basic idea of MTDL is based on a “one for all” concept, which could be achieved by screening for unexplored synthetic or natural molecules and biomacromolecular structures, which possess intrinsic multitarget properties and also enhance activity of already known drugs by modifying their structure.

Almost 10 years ago, Gökhan-Kelekçi et al. reported that appropriate modification of 4(3H)-quinazolinone can lead to agents against neurodegenerative diseases. Several authors were inspired by this work and designed novel derivatives with antidepressant, antioxidant, antiamyloid, and dual cholinesterase inhibitory activity.²² 2,4-Disubstituted quinazoline ring scaffold was shown to possess multitarget activities. Effective quinazoline derivatives exhibited dual cholinesterase inhibition and antioxidant activity and were able to inhibit formation of A $\beta_{40/42}$ aggregates with IC₅₀ values in low micromolar range.²³ Also, quinazolinone-hydrazone derivatives were investigated as new multitarget candidates for the treatment of AD. The compounds containing a 2,3-dichlorophenyl and 2,4-dihydroxyphenyl moieties showed the highest activity with an IC₅₀ value against BACE1 in micromolar range and a significant antioxidant effect using 2,2-diphenyl-1-picrylhydrazyl (DPPH) assay.²⁴ Kroth et al. designed novel 2,6-disubstituted pyridine derivatives able to interact with the β -sheet conformation of A β and thus inhibit A β_{42} aggregation. The 2,6-diaminopyridine moiety was identified as a key component in the design of potential inhibitors of A β_{42} fibrils formation.²⁵ Moreover, pyridine derivatives with carbamic or amidic functional groups have been synthesized to inhibit cholinesterase activity and inhibit A β_{42} amyloid aggregation.²⁶

In our previous study,²⁷ using an efficient protocol that combines steered molecular dynamics (SMD) with experimental data on binding affinity of reference compounds, we tried to obtain multitarget AD drug candidates from the large PubChem database (<https://pubchem.ncbi.nlm.nih.gov>). We have found two compounds, CID 16040294 (GVD, 2-[4-([17]amino)phenyl]acetonitrile) and CID 9998128 (N-(1H-indazol-5-yl)-2-(6-methylpyridin-2-yl) quinazolin-4-amine), which display high binding affinity to six targets including A β fibril, peroxisome proliferator-activated receptor γ (PPAR γ), retinoic X receptor α (RXR α), β - and γ -secretases and acetylcholinesterase (AChE).

In this study, we have experimentally confirmed *in silico* predicted multipotent effect of CID 9998128 to influence various targets associated with AD. We have focused on the effect of CID 9998128 on three AD targets, namely, A β_{42} peptide, A β_{42} fibrils, and β -secretase. The intensive inhibitory effect of CID 9998128 was observed for amyloid fibrillogenesis and β -secretase activity. Moreover, CID 9998128 is capable of effective clearance of A β_{42} amyloid fibrils. The multitarget relative binding affinity of CID 9998128 was theoretically examined by SMD, but its absolute value has not been computed.²⁷ Thus, our second goal of this study is to estimate the binding free energy of CID 9998128 to A β_{42} fibril and β -secretase using the molecular mechanics Poisson–Boltzmann surface area (MM-PBSA) method. Both *in vitro* and *in silico* experiments showed that CID 9998128 is strongly bound to these targets suggesting that it can serve as a prominent candidate for AD multitarget treatment.

RESULTS AND DISCUSSION

Docking Simulation. For the purpose of this study, the structure of CID 9998128 (Figure 1) was divided to three structural blocks: quinazoline (block 1), indazole (block 2), and methylpyridine (block 3) functional groups.

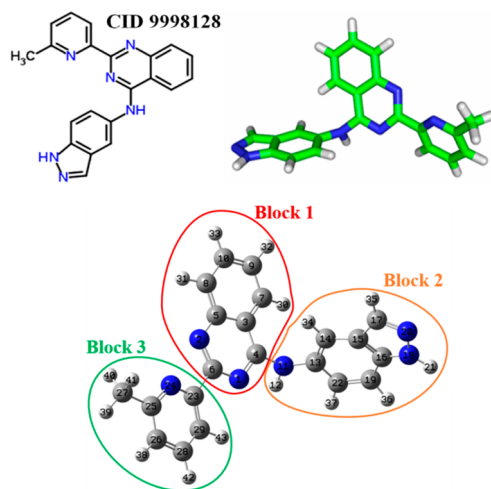


Figure 1. The 2D and 3D structure of CID 9998128. The structure of CID 9998128 was divided into three structural blocks: quinazoline (block 1), indazole (block 2), and methylpyridine (block 3) functional groups. All atoms are numbered.

For our simulation, we used the NMR structures 2MXU and 2NAO obtained for truncated fragment $\text{A}\beta_{11-42}$ and full length $\text{A}\beta_{1-42}$, respectively.^{28,29} The crystal structure of β -secretase

1M4H was obtained by the X-ray diffraction method.³⁰ The used atomic structures of targets together with the position of CID 9998128 in the best docking mode are shown in Figure 2. The positions of CID 9998128 in the 5 best docking modes in 2NAO are also shown in Figure S1 in Supporting Information (SI). Clearly, this ligand prefers to stay near the N-terminus of one sheet and strongly interacts with it. As seen below, this behavior remains the same in our MD simulation.

The docking binding energies between CID 9998128 and 2MXU, and also between CID 9998128 and 1M4H are described in our previous paper²⁷ and are equal to -9.7 kcal/mol (2MXU) and -9.8 kcal/mol (1M4H), respectively. For 2NAO target, the present simulation gives $\Delta E_{\text{bind}} = -8.9 \text{ kcal/mol}$ showing that the binding energy is nearly equal for three targets. Details on the best binding mode of CID 9998128 to 2MXU and 1M4H are available in ref 27. Briefly, CID 9998128 has no hydrogen bonds (HBs) and 15 nonbond contacts with 2MXU.²⁷ The situation is different for β -secretase (1M4H) target, which forms 3 HBs and 9 nonbond contacts with CID 9998128.²⁷ In the 2NAO case, CID 9998128 is bound to the N-termini of D, E, and F chains (Figure 2). By LigPlot⁺ version 1.4.5, one can show that no hydrogen bonding occurs between CID 9998128 and 2NAO but 12 nonbonded contacts are formed with His13(E), Gly9(F), His6(E), His6(F), Phe4(F), Phe4(E), His6(D), Val12(D), Phe4(D), Tyr10(D), Val12(E), and Gly9(E) (Figure 3). Thus, it has 7 bonds with hydrophobic amino acids (Gly, Phe, Val), 4 bonds with basic His, and one bond with polar Tyr, pointing to dominance of the interaction with hydrophobic residues. Although there are no hydrogen bonds between the ligand CID 9998128 and 2NAO in docking, they occasionally appear during MD simulation as shown

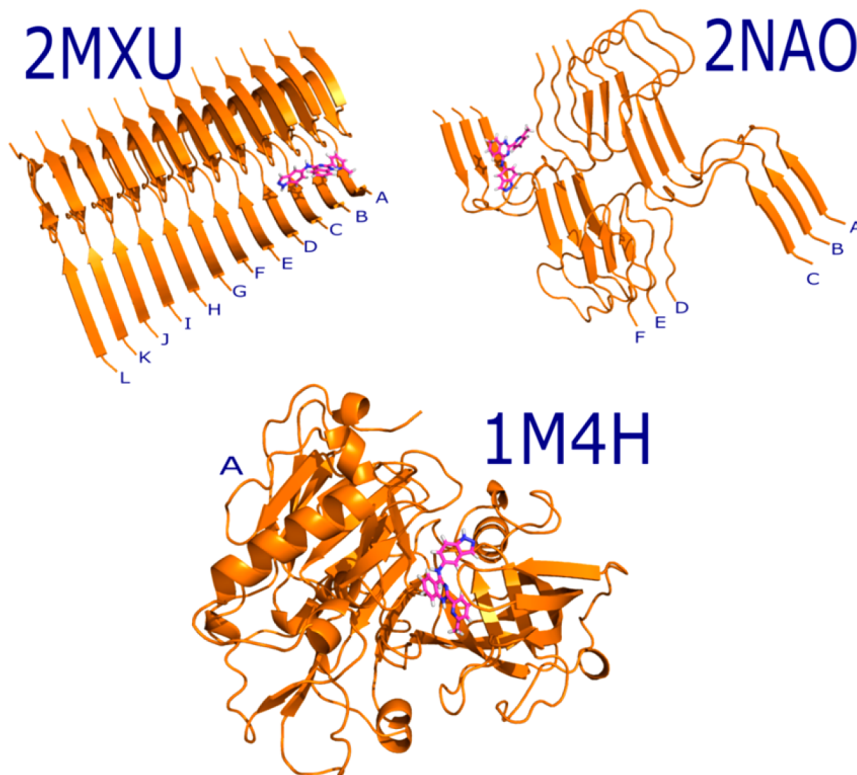


Figure 2. Position of compound CID 9998128 in the best docking mode for 2MXU, 2NAO, and 1M4H. Capital letters, which denote polypeptide chains, are located either at the 11th and 42nd residue in case of truncated fragment $\text{A}\beta_{11-42}$ (2MXU), or 1st and 42nd residue for full length $\text{A}\beta_{1-42}$ peptide (2NAO).

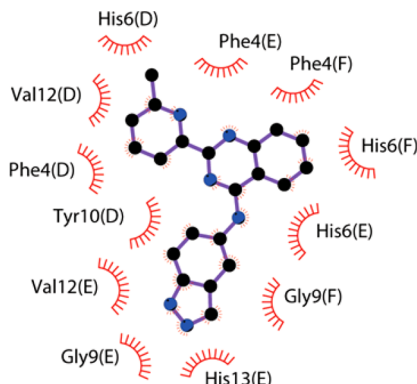


Figure 3. Nonbonded contacts of CID 9998128 with a full length $\text{A}\beta_{1-42}$ (2NAO) in the best docking mode. No hydrogen bond was observed.

below. Taken together, in docking simulation, nonbonded contacts dominate over the hydrogen bonding in stability of all studied complexes.

MM-PBSA Results. Estimation of Binding Free Energy. Because docking results are not reliable enough due to several crude approximations, they have been further refined using the more accurate MM-PBSA method. For each complex, we have conducted 4 independent 100 ns MD trajectories employing the same configuration obtained in the best docking mode (Figure 2) as initial configuration but with different random seed numbers.

We monitored the time dependence of RMSD and assumed that the system reached equilibrium when RMSD reaches saturation fluctuating around its equilibrium value. It is evident from Figures S2–S4 in Supporting Information (SI) that $\text{A}\beta_{1-42}$ (2MXU) + CID 9998128 and $\text{A}\beta_{1-42}$ (2NAO) + CID 9998128 complexes reach equilibrium after about 40–60 ns, while the equilibration time of β -secretase (1M4H) + CID 9998128 complex is about 40 ns. Snapshots collected every 10 ps at equilibrium were used to estimate ΔG_{bind} using eq 1. The results obtained for each MD run are shown in Tables S1–S3 in SI. Averaging over 4 trajectories, we obtained the binding free energy, which is almost the same for full-length and truncated fibrils (Table 1). But, it is a bit lower for β -secretase having $\Delta G_{\text{bind}} \approx -18.8$ kcal/mol. Consistent with results obtained by steered MD,²⁷ MM-PBSA method also ascertains that CID 9998128 is a good binder both to $\text{A}\beta$ fibrils and to β -secretase. However, the advantage of MM-PBSA is that it can predict the absolute binding free energy instead of relative binding affinity in SMD simulation.

It is evident from Table 1 that the absolute value of the vdW term is higher than the electrostatic one implying that the vdW interaction is more important than the electrostatic interaction in binding of CID 9998128 toward three targets. Note that the

dominance of vdW interaction is observed for the whole simulation time (Figure S5).

Per-residue distributions of the interaction energy of $\text{A}\beta_{1-42}$ fibril (2MXU) with CID 9998128 (Figure S6) show that residues 12, 14, 17, 19, and 32–34 make the main contribution to the vdW interaction, while residues 14, 28, and 42 are important for the electrostatic interaction. The situation is different for the $\text{A}\beta_{1-42}$ fibril (2NAO) case (Figure S7), where residues at the N-terminus of one S-sheet of three chains, in particular, residues 4 and 6 are the driving force in ligand binding. A small contribution comes from a few residues at the C-terminus of the second sheet.

In order to shed more light on binding mechanisms, the structure of CID 9998128 was divided into three blocks, each of which contains at least one aromatic ring (Figure 1). Blocks 1, 2, and 3 have 14, 16, and 13 atoms, respectively. Names, types, masses, and charges of atoms are shown in Table S4.

Having two rings, blocks 1 and 2 equally contribute to the vdW interaction with both fibrillar targets 2MXU and 2NAO (Table S5). Block 3 behaves differently as its vdW interaction with 2MXU (-14.1 kcal/mol) is more favorable than that with 2NAO (-7.9 kcal/mol). For 1M4H, the contribution to vdW interactions from all 3 blocks is almost the same (about -11.0 kcal/mol).

Due to different total charges, the three blocks contribute differently to the electrostatic interaction. Positively charged blocks 1 and 3 have an attractive interaction with the three targets, while negatively charged block 2 experiences repulsion (Table S5). The interaction strength largely depends on the targets. Block 1 makes a significant contribution to electrostatic interaction with 2NAO (-25.8 kcal/mol) compared to the remaining targets (about -5.5 kcal/mol). Indazole (block 2) substantially destabilizes both 2NAO + CID 9998128 and 1M4H + CID 9998128 complexes through repulsive Coulomb interaction (+25.4 and +4.0 kcal/mol, for 2NAO + CID 9998128 and 1M4H + CID 9998128, respectively) (Table S5), while block 3 stabilizes β -secretase. Based on this observation, we predict that the structure of potential multitarget drugs for AD should not contain indazole.

Nonbonded Contacts (NBCs) Dominate over Hydrogen Bonding. Figure S5 shows the time dependence of the number of HBs (N_{HB}) in MD simulation for 3 targets. Averaging over 4 trajectories, we obtain mean $N_{\text{HB}} = 0.5, 1.4$, and 1.6 for 2MXU, 2NAO, and 1M4H, respectively (Table S6). The hydrogen bonding of CID 9998128 with β -secretase is a little bit stronger than that with $\text{A}\beta$ fibrils presumably because it resides in the deep binding site of 1M4H (Figure 2 and Movie 1). For truncated 2MXU fibril, CID 9998128 forms a HB with 7 residues from different chains including His14(B), Glu11(D), His14(A), Ile32(E), Gly33(D), Glu11(A), and Leu34(E) (Table S1). In the full-length 2NAO fibril, 4 additional residues

Table 1. Binding Free Energy ΔG_{bind} (kcal/mol), Estimated by the MM-PBSA Method, for CID 9998128 to Truncated $\text{A}\beta_{11-42}$ (2MXU) and Full Length $\text{A}\beta_{1-42}$ (2NAO) Fibrils and β -Secretase (1M4H)^a

	ΔE_{ele} (kcal/mol)	ΔE_{vdw} (kcal/mol)	ΔG_{PB} (kcal/mol)	ΔG_{sur} (kcal/mol)	$-T\Delta S$	ΔG_{bind}
2MXU	-7.4 ± 0.8	-43.2 ± 2.7	26.6 ± 2.2	-6.0 ± 0.3	7.7 ± 1.1	-22.4 ± 0.6
2NAO	-9.1 ± 1.2	-38.9 ± 5.0	21.6 ± 4.9	-5.4 ± 0.6	8.4 ± 1.3	-23.4 ± 1.8
1M4H	-17.7 ± 1.2	-32.8 ± 1.0	31.0 ± 0.8	-5.6 ± 0.1	6.3 ± 0.5	-18.8 ± 1.1
$\text{A}\beta_{1-42}$ monomer	-14.2	-34.0	20.1	-4.6	7.9	-24.8 ± 1.8
$\text{A}\beta_{1-42}$ dimer	-13.7	-26.6	17.0	-3.8	5.3	-21.8 ± 2.9

^avdW interaction is more important than electrostatic interaction and the role of indazole (second block).

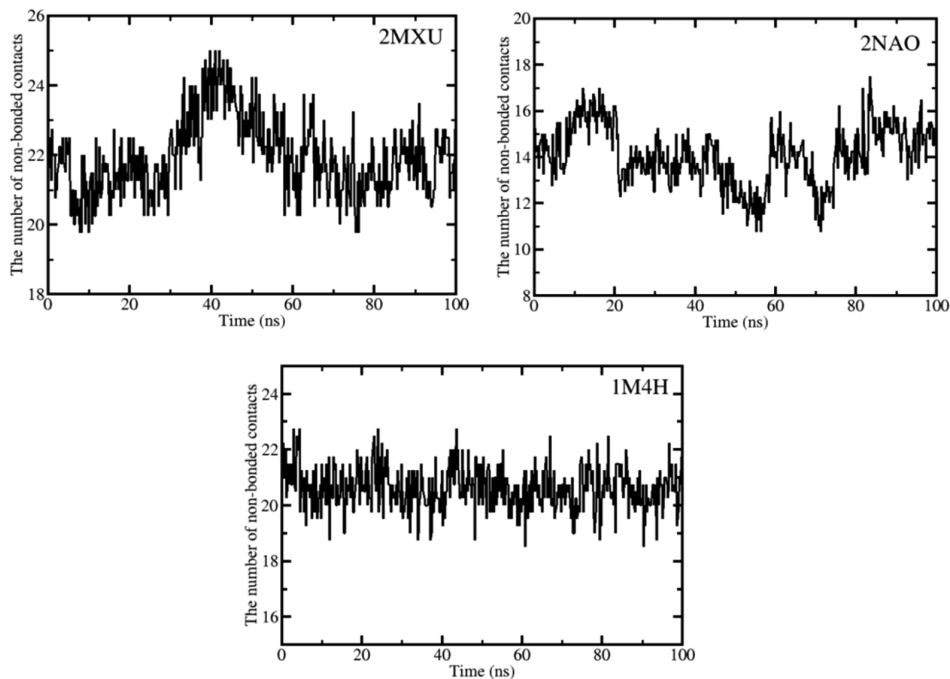


Figure 4. Time dependence of the number of nonbonded contacts (NBCs) between CID 9998128 and three targets in MD simulation. Results were averaged over 4 trajectories.

are involved in the HB network resulting in the higher mean number of HBs (1.4) compared to the 2MXU case (0.5). During MD simulation, CID 9998128 forms HBs with 11 residues from the binding site of β -secretase (Table S6). Because N_{HB} remains below 2 in all cases, in agreement with docking results, the HB network remains poor in MD simulation.

As is evident from Figure 4, fluctuations of the number of nonbonded contacts (N_{NBCs}) between the ligand and β -secretase are less than those of fibril targets 2MXU and 2NAO because the movement of CID 9998128 in the 1M4H binding site is more confined compared to the latter cases. This is also clear if one compares Movie 1 with Movie 2 (SI) as CID 9998128 moves near the hydrophobic region of 2NAO. Averaging over 4 MD runs, we obtain $N_{\text{NBCs}} = 21.9$, 14.1, and 20.6 for 2MXU, 2NAO, and 1M4H, respectively (Table S6). Thus, the number of HBs is significantly lower than nonbonded contacts during MD implying that NBCs play a major role in binding affinity of CID 9998128. Table S6 also shows residues that form NBCs with CID 9998128 during MD course at equilibrium for all targets. For 2NAO, for instance, CID 9998128 prefers to stay near the N-terminus of chains D, E, and F and occasionally interacts with the residues from the C-termini of chains A, B, and C. This result is consistent with the analysis of per-residue distributions of the vdW and electrostatic interactions (Figure S7).

The fact that the binding affinity of CID 9998128 to $A\beta_{11-42}$ and $A\beta_{1-42}$ fibrils, obtained in our *in silico* experiment (Table 1), is nearly the same does not mean that the 1–10 region has no effect. Instead, we have clearly shown that CID 9998128 mainly interacts with the N-terminus (Movie 2 and Figure S7). Therefore, mutations at this terminus like A2V, A2T,^{31–33} D7H,^{34,35} and D7N^{36,37} may alter the impact of CID 9998128 on fibrillation pathways and rate.

Binding Free Energy of CID 9998128 to $A\beta_{1-42}$ Monomer. In order to understand the molecular mechanism of fibril

growth in the presence of ligand, we have studied the binding affinity of CID 9998128 toward $A\beta_{1-42}$ monomer and dimer. Because $A\beta_{1-42}$ monomer does not have a well-defined native structure, we first docked the ligand to the 9 most populated structures obtained in all-atom MD simulation (Figure S9).³⁸ Using these structures as initial structures, we have carried out 4 independent 200 ns MD simulations for each of them. As evident from the time dependence of RMSD (Figure S10), the equilibration varies between 80 and 160 ns depending on complex and MD run.

The results of MM-PBSA calculation at equilibrium are shown in Table S7 (see also Table 1). Clearly, CID 9998128 strongly binds to the monomer ($\Delta G_{\text{bind}} = -24.8$ kcal/mol) preventing the fibril formation. This is in the line with our *in vitro* experiment. As in the fibril case, the vdW interaction dominates over the electrostatic one. As follows from per-residue distributions of the interaction energy (Figure S8), CID 9998128 interacts with the N-terminus more strongly than with the C-terminus. The weakest interaction occurs near the turn region. The interaction energy profile (Figure S11) also indicates that CID 9998128 does not have a well-defined binding site but rather travels around the target during simulation. Similar behavior was also observed for curcumin interacting with $A\beta_{1-42}$ monomer.³⁹

Binding Free Energy of CID 9998128 to $A\beta$ Dimer. The structure of $A\beta_{1-42}$ dimer⁴⁰ with CID 9998128, obtained in the best docking mode, has been used as a starting configuration for MD simulation (Figure S12). Using different random seed numbers, we have performed four 100 ns independent MD trajectories. The time dependence of RMSD with respect to the initial structure of dimer shows that the complex reaches equilibrium at about 50 ns (Figure S13). The equilibration time of the dimer complex is shorter than that of monomer (Figure S10) because the dimer is less flexible.

The contribution from an individual MD trajectory to the equilibrium binding free energy is shown in Table S8. As in the

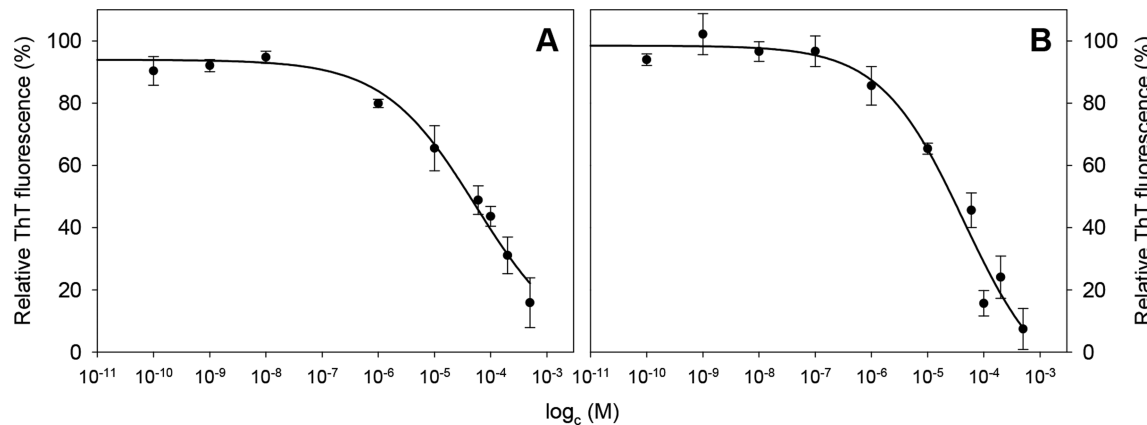


Figure 5. Dose-dependent effect of CID 9998128 on $A\beta_{1-42}$ fibril formation (A) and $A\beta_{1-42}$ fibrils (B) monitored by ThT fluorescence assay. The fluorescence intensities of samples were normalized to the fluorescence intensities of 10 μM amyloid fibrils alone (taken as 100%). The experiment was performed in triplicate, and presented data represent average values with standard deviation.

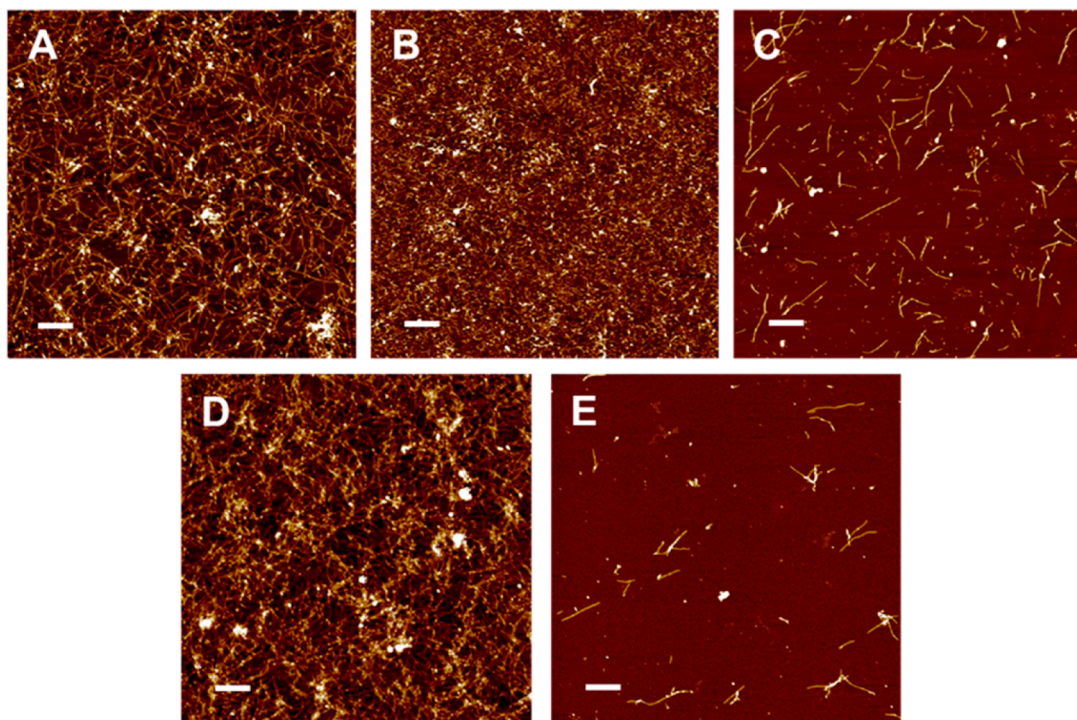


Figure 6. Representative AFM images of 10 μM $A\beta_{1-42}$ fibrils formed alone (A) or in the presence of 1 μM (B) or 100 μM (C) compound CID 9998128; effect of 1 μM (D) or 100 μM (E) compound CID 9998128 on mature $A\beta_{1-42}$ fibrils after 24 h incubation. The scale bars represent 1 μm .

case of monomer and fibril CID 9998128 strongly binds to dimer ($\Delta G_{\text{bind}} = -21.8$ kcal/mol) suggesting that in the presence of this compound the oligomerization/fibrillization process slows down, in agreement with our *in vitro* experiment.

One has to stress that the binding mechanism to dimer is different from monomer (compare Figures S11 and S14) because in dimer CID 9998128 weakly interacts with the N-terminus. Residues 17–20, 28, 34, and 35 are crucial in controlling binding affinity.

Antiamyloid Activity of CID 9998128. The *in vitro* amyloid self-assembly of $A\beta_{1-42}$ peptide to fibrils in the presence of compound CID 9998128 and its effect on amyloid fibrils were studied by following the changes in ThT fluorescence intensities and morphological characteristics. ThT fluorescence assay is a routine method for monitoring amyloid aggregation processes. The compound CID 9998128 in a broad

concentration range from 100 pM to 1 mM was added to 10 μM $A\beta_{1-42}$ monomer solution, and formation of amyloid fibrils was observed after 8 days incubation (Figure 5A). The decrease in ThT fluorescence signals signifies the inhibition of the process in the presence of increasing compound concentration. We also examined the effect of CID 9998128 on $A\beta_{1-42}$ fibrils at the same concentration range after 24 h incubation. As is shown in Figure 5B, a significant reduction in the fluorescence intensities was observed in a concentration dependent manner. The obtained data indicate that CID 9998128 is able to dose-dependently dissociate $A\beta_{1-42}$ amyloid fibrils. To validate the inhibition and dissociation effect of studied compound, the IC₅₀ and DC₅₀ values (the concentration of compound with half-maximal inhibitory/dissociate activity) were determined. The obtained IC₅₀ and DC₅₀ values were in micromolar range and are equal to 42.6 and 22.7 μM , respectively.

Atomic force microscopy was exploited to directly visualize morphological changes in amyloid fibrils after affecting fibrilization of $A\beta_{1-42}$ peptide with compound CID 9998128. Dissociation of mature $A\beta_{1-42}$ amyloid fibrils facilitated by compound CID 9998128 was also visualized (Figure 6). The untreated $A\beta_{1-42}$ fibrils shown in Figure 6A have well-defined fibrillar structures with typical amyloid morphology. Addition of 1 μM CID 9998128 had no significant effect on amyloid self-assembly of $A\beta_{1-42}$ regarding their amount and morphology (Figure 6B). On the other hand, 100 μM compound concentration led to considerable decrease in amount of fibrils and formation of shorter fragments was observed (Figure 6C). In relation to dissociation efficiency, after treatment of mature fibrils with 1 μM CID 9998128, no significant changes in morphology and amount of fibrillar aggregates were observed (Figure 6D). Meanwhile, incubation of fibrils with 100 μM compound concentration induced clearance of long fibrils, and only a small amount of short fragments was present (Figure 6E).

Inhibition of β -Secretase Activity. β -Secretase has a critical role in $A\beta$ peptide generation and its concentration is elevated in the brains of AD patients. Recently, β -secretase is considered as a prime drug target for inhibition of $A\beta$ production.⁴¹ Therefore, we have studied the potential of compound CID 9998128 to bind to the enzyme and thereby decrease its activity (Figure 7). The inhibitory activity is expressed as EC_{50} value (the inhibitor concentration with 50% decrease in enzyme activity) of 15 μM .

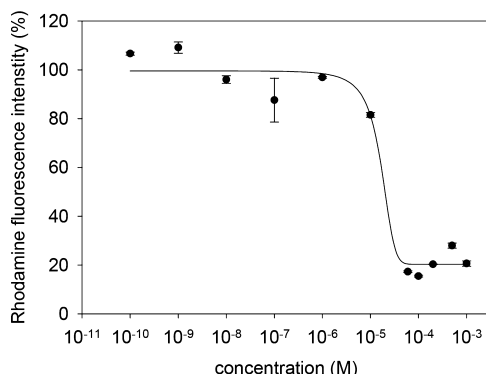


Figure 7. Effect of compound CID 9998128 on β -secretase activity determined as rhodamine fluorescence using FRET assay. The error bars represent standard deviation from average values of three independent samples.

The recent approach to discover more effective and safer therapies for AD aims to use multitarget hybrid small molecules that target multiple pathological factors involved in AD. It is believed that it is a right concept when dealing with disease as complex and multifaceted as AD. Since then, several papers were published regarding applying this approach for drug design.^{42–44} It has been shown that donepezil, tacrine, curcumin, and rivastigmine are potential pharmacophoric scaffolds for molecular hybridization. Tacrine is well-known for its remarkable potency to interact with acetylcholinesterase. Therefore, Martins et al. designed a new series of tacrine derivatives by the insertion of a furo[2,3-*b*]quinolin-4-amine and pyrrolo[2,3-*b*]quinolin-4-amine subunits.⁴⁵ The lead compounds have the inhibitory activity in low nanomolar range and significant neuroprotective effect against $A\beta$ -induced toxicity. Molecular modeling studies pointed out that the

derivatives containing pyrrole substituted with phenyl ring at the position 1 interacts with AChE and BuChE in greater manner. Hamulakova et al.⁴⁶ demonstrated that novel designed and synthesized multifunctional tacrine–coumarine hybrids have antioxidant and copper-chelating properties and protective effects against DNA damage caused by free radicals. Moreover, the hybrids inhibit activities of acetylcholinesterase and butyrylcholinesterase and amyloid aggregation of $A\beta$ peptide.

Based on multitarget approach Mohamed and collaborators developed a novel library of quinazoline derivatives as multitargeting agents against Alzheimer's disease. 2,4-Disubstituted derivatives exhibit cholinesterase inhibition and antioxidant properties. Several compounds exhibited varying levels of $A\beta_{40}$ and $A\beta_{42}$ peptide aggregation inhibition.²³ Several biochemical studies have shown that heterocyclic compounds with indazole ring scaffold are potent γ -secretase modulators.⁴⁷ These results strengthen our belief that compound CID 9998128, the structure of which contains both of above-mentioned scaffolds, could be used as potential MTDL agent.

CONCLUSION

Using *in vitro* and *in silico* methods, we have tested compound CID 9998128 as a potential multitarget drug against targets associated with AD, such as $A\beta_{42}$ peptide and its fibrillar state as well as β -secretase. Binding mechanisms were studied at the atomic level demonstrating that the vdW interaction plays an important role. The second block of CID 9998128, which contains indazole, makes a major contribution to instability of three studied complexes due to repulsive interaction with the receptor. From this perspective, we suggest that the chemical structure of multitarget AD leads should not have indazole. However, more work should be done to cement our prediction.

By *in vitro* experiments, we have shown that the compound dose-dependently inhibits formation of $A\beta_{1-42}$ amyloid fibrils. Moreover, CID 9998128 is able to clear $A\beta_{1-42}$ fibrils in a concentration dependent manner. The obtained IC_{50} and DC_{50} values are in the micromolar range indicating significant anti-amyloid activities of the compound within stoichiometric concentration with $A\beta_{1-42}$ peptide and amyloid fibrils. The atomic force microscopy confirmed that the presence of CID 9998128 led to significant decrease of the amount of the fibrils and their morphological changes, as only short fragments were observed. Intensive interference was also determined for CID 9998128 with another target, β -secretase. It was found that the compound significantly decreased β -secretase activity due to its binding to this enzyme. The obtained EC_{50} value is in micromolar range. The obtained data suggest that compound CID 9998128 represents a prominent candidate for multitarget treatment of Alzheimer's disease due to ability to hit multiple targets.

Finally, from the methodology point of view one has to stress that the strong binding of CID 9998128 to $A\beta$ monomer, oligomer, and fibril means that it can either interfere with or promote fibril growth. In order to establish its inhibitory/anti-inhibitory effect one has to perform complementary MD simulations or *in vitro* experiments. In this paper, we have made the second choice having carried out the ThT fluorescence assay and AFM experiment, which show that CID 9998128 can not only clear up $A\beta$ fibrils but also interfere with the fibril growth.

METHODS

Molecular Simulation. *Ligand and Receptors.* The atomic structure of CID 9998128 is shown in Figure 1. To mimic $\text{A}\beta_{42}$ fibrils we used the solid state NMR structure obtained for truncated fragment $\text{A}\beta_{11-42}$ with PDB code 2MXU²⁸ and the structure of full length $\text{A}\beta_{1-42}$ with PDB code 2NAO.²⁹ Although other experimental $\text{A}\beta_{42}$ fibrillar structures are available,⁴⁸ these S-shape structures achieved independently by two groups are very likely reliable.⁴⁹

Similar to our previous papers^{50,51} to estimate the binding free energy of CID 9998128 to monomer, we used 9 representative structures (Figure S9 in SI), obtained by all-atom MD simulation,³⁸ as binding targets.

The *in silico* structure of $\text{A}\beta_{1-42}$ dimer has been proposed by several groups.^{40,52,53} However, in our simulation, we have used the structure obtained by Zhang et al.⁴⁰ (Figure S12 in SI) because it was supported by AFM experimental data.

The crystal structure of β -secretase obtained by the X-ray diffraction method with PDB ID 1M4H³⁰ was employed for simulation. The atomic structures of three targets are shown in Figure 2.

Molecular Dynamics Simulation. The force field AMBER-f99SB-ILDN,⁵⁴ which is reasonable for $\text{A}\beta$ simulation,^{53,55} and water model TIP3P⁵⁶ was utilized in MD simulation. Force field parameters of ligand were computed using Antechamber⁵⁷ and Acpcpe⁵⁸ based on the General Amber Force Field (GAFF).⁵⁹ The atomic point charges were defined by the AM1-BCC.⁶⁰ Parameters used for CID 9998128 simulation were presented in our previous paper.²⁷

For van der Waals (vdW) forces calculation, the cutoff of 1.42 nm was adopted. The same cutoff was chosen to compute the electrostatic energy using the particle-mesh Ewald (PME) summation method.⁶¹ The leapfrog algorithm⁶² was employed to solve the corresponding Langevin equations. Every 10 fs, we updated the pair-list for long-range interactions using the cutoff of 1.0 nm. To neutralize the system, 12, 18, and 9 Na^+ ions were added to 2MXU, 2NAO and 1M4H, respectively.

After energy minimization with the steepest descent method,⁶³ we performed position-restrained simulations for 500 ps allowing water molecules to get into the binding site. The Berendsen algorithm⁶⁴ and damping coefficient 0.1 ps were used to keep temperature 300 K constant during 500 ps NVT simulation. For production of NPT runs at 300 K and 1 atm, the Parrinello–Rahman coupling⁶⁵ was employed with damping coefficient 0.5 ps.

Molecular Mechanics- Poisson–Boltzmann Surface Area (MM-PBSA) Method. The binding free energy, ΔG_{bind} , has the following terms by Molecular Mechanics Poisson–Boltzmann Surface Area (MM-PBSA) method⁶⁶ (more details on this method may be found elsewhere^{38,67}):

$$\Delta G_{\text{bind}} = \Delta E_{\text{elec}} + \Delta E_{\text{vdW}} + \Delta G_{\text{sur}} + \Delta G_{\text{PB}} - T\Delta S \quad (1)$$

where ΔE_{elec} and ΔE_{vdW} are electrostatic and vdW interaction energies. ΔG_{PB} and ΔG_{sur} are polar and nonpolar solvation energies. The entropy change ΔS was computed by the interaction entropy method proposed recently by Duan et al.⁶⁸

Definition of Relevant Quantities. RMSD (root-mean-square deviation) is defined as the deviation of receptor backbone from its starting structure. Hydrogen bond (HB) occurs if D (donor)–A (acceptor) distance is ≤ 3.5 Å, H–A distance is ≤ 2.7 Å, and D–H–A angle is $\geq 135^\circ$. If the distance between centers of mass of ligand and some receptor residue is within 0.65 nm, then we assume that a nonbonded contact is formed.

Experimental Methods. *Chemicals.* Human β -amyloid (1–42) peptide ($\text{A}\beta_{1-42}$ peptide) was purchased from rPeptide company (USA), β -secretase (BACE-1) FRET Assay Kit was obtained from Pan Vera's, WI, USA. Hydrochloric acid, thioflavin T (ThT), dimethyl sulfoxide (DMSO), and hexafluoroisopropanol (HFIP) were purchased from Sigma-Aldrich (USA) and were of analytical grade. Studied compound CID 9998128 (*N*-(1*H*-indazol-5-yl)-2-(6-methyl-pyridin-2-yl) quinazolin-4-amine) was from Ottawa Chemicals (Canada).

Formation of $\text{A}\beta_{1-42}$ Peptide Amyloid Fibrils. Human $\text{A}\beta_{1-42}$ peptide was pretreated with HFIP. The $\text{A}\beta_{1-42}$ peptide film was dissolved in 100% DMSO to a 5 mM concentration. This stock solution was centrifuged at 14 000g for 30 s and sonicated in a bath sonicator at 4 °C for 10 min. Afterward the stock solution was diluted to 10 μM (for experiments with $\text{A}\beta_{1-42}$ monomer) or 100 μM solution (experiments with $\text{A}\beta_{1-42}$ fibrils) in 10 mM HCl buffer (pH 2.4) and incubated 8 days at 37 °C. Presence of amyloid fibrils was confirmed using several techniques such as thioflavin T assay and atomic force microscopy.

Thioflavin T (ThT) Fluorescence Assay. The extent of $\text{A}\beta_{1-42}$ fibril formation was quantified using fluorescent probe ThT. Its fluorescence is significantly enhanced after binding to amyloid fibrils. ThT was added to the samples containing 10 μM $\text{A}\beta_{1-42}$ solution to a final concentration of 20 μM . Samples were incubated at 37 °C for 1 h in the dark. The ThT fluorescence intensity was recorded at 485 nm after sample excitation at 440 nm in 96-well black plates using spectrofluorimeter Synergy Mx (BioTek, USA). The excitation and emission slits were set to 9.0/9.0 nm. All experiments were performed as three independent samples, and the presented values are the average of measured values.

Effect of CID 9998128 Compound on $\text{A}\beta_{1-42}$ Peptide Amyloid Fibrillization and Amyloid Fibrils: Determination of IC_{50} and DC_{50} Values. The interference of compound CID 9998128 with amyloid aggregation processes of $\text{A}\beta_{1-42}$ peptide was studied using ThT assay. Effect of compound in concentration range from 1 mM to 100 pM on $\text{A}\beta_{1-42}$ peptide fibril formation (10 μM) was examined after 8 days incubation and on $\text{A}\beta_{1-42}$ fibrils after 24 h incubation at 37 °C. As a positive control, the compound was replaced in samples with buffer. As a negative control, protein was replaced with buffer and fluorescence of compound was measured. All recorded fluorescence intensities were normalized to the ThT fluorescence intensities measured for $\text{A}\beta_{1-42}$ aggregates alone (100%). Each experiment was performed in three separate samples, and the final value represents the average of measured data. The IC_{50} and DC_{50} values (concentration of compound CID 9998128 with 50% inhibiting or destroying activity) were calculated from concentration dependencies fitted with the nonlinear least-squares method using SigmaPlot software.

Atomic Force Microscopy (AFM). Samples containing $\text{A}\beta_{1-42}$ aggregates alone or formed in the presence of different concentrations of compound were placed on freshly cleaved mica by drop casting method and left to adsorb on the surface for 5 min. The surface was then rinsed with ultrapure water several times and dried under nitrogen gas. AFM images were collected using scanning probe microscope (Veeco di Innova) in tapping mode with 512 × 512 pixels resolution. A rectangular uncoated silicon cantilever, NCHV (Bruker AFM Probes), with a specific resistance of 0.01–0.025 Ω cm and typical resonance frequency 320 kHz was used. No further smoothing or noise reduction was applied.

Interference of CID 9998128 Compound with β -Secretase Activity. The effect of CID 9998128 on β -secretase activity was tested using β -secretase (BACE1) FRET Assay Kit. The mixture containing 250 nM BACE1 substrate (rhodamine-EVNLDAEFK-quencher), 10 milliunits of BACE1 enzyme, and serially diluted compound (concentration range from 100 pM to 1 mM) in 50 mM sodium acetate buffer was incubated for 90 min at room temperature in the dark. Rhodamine fluorescence was recorded using 96-well half area microplates (Corning, NY, USA) on a Synergy Mx spectrofluorimeter with excitation wavelength of 545 nm and maximal emission at 585 nm. The excitation and emission slits were set at 13.5 nm. Error bars represent standard deviation from average values of three independent measurements.

ASSOCIATED CONTENT

S Supporting Information

The Supporting Information is available free of charge on the ACS Publications website at DOI: 10.1021/acscchemneuro.0b00091.

Data on binding free energy of CID 9998128 to $\text{A}\beta_{42}$ and β -secretase, time dependence of RMSD of target + CID 9998128 complexes, of the electrostatics and van der Waals interaction energies between CID 9998128 and three targets, and of the number of HBs formed by CID 9998128 with target during MD simulation ([PDF](#))
 Movement of CID 9998128 around full-length 2NAO fibril during MD simulation ([MPG](#))
 Movement of CID 9998128 in the binding site of β -secretase at equilibrium ([MPG](#))

AUTHOR INFORMATION

Corresponding Authors

*Z.G. E-mail: gazova@saske.sk.
 *M.S.L. E-mail: masli@ifpan.edu.pl.
 *C.-K.H. E-mail: huck@phys.sinica.edu.tw.

ORCID

Mai Suan Li: [0000-0001-7021-7916](https://orcid.org/0000-0001-7021-7916)
 Zuzana Gazova: [0000-0002-0670-3431](https://orcid.org/0000-0002-0670-3431)

Author Contributions

◆ N.Q.T. and Z.B. contributed equally. N.Q.T. and H.Q.L performed *in silico* calculations. M.S.L. designed *in silico* experiments. Z.B. and M.G. designed and performed *in vitro* experiments. Z.B. analyzed data. Ch.-K.H., M.S.L., and Z.G. wrote the manuscript with help from Z.B.

Notes

The authors declare no competing financial interest.

ACKNOWLEDGMENTS

This work was supported by the research grant projects in frame of VEGA 2/0145/17, 2/0030/18, SF EU 2622012033, MVTS COST 083/14 action BM1405, and SAS-MOST JRP 2015/S. This research was supported by Institute for Computational Science and Technology (Grant No. 13/2017/HĐ-KHCNTT) and Department of Science and Technology at Ho Chi Minh City, Vietnam. C.-K.H. was supported by Grants MOST 105-2112-M-001-004 and MOST 106-2112-M-001-027. M.S.L. was supported by the Polish NCN grant 2015/19/B/ST4/02721, Poland.

REFERENCES

- (1) Xu, Y., Yan, J., Zhou, P., Li, J., Gao, H., Xia, Y., and Wang, Q. (2012) Neurotransmitter receptors and cognitive dysfunction in Alzheimer's disease and Parkinson's disease. *Prog. Neurobiol.* 97, 1–13.
- (2) Selkoe, D. J., and Hardy, J. (2016) The amyloid hypothesis of Alzheimer's disease at 25 years. *EMBO Mol. Med.* 8, 595–608.
- (3) Murphy, M. P., and LeVine, H., III (2010) Alzheimer's disease and the amyloid- β peptide. *J. Alzheimer's Dis.* 19, 311–323.
- (4) Vassar, R. (2002) β -secretase (BACE) as a drug target for Alzheimer's disease. *Adv. Drug Delivery Rev.* 54, 1589–1602.
- (5) Yan, R., and Vassar, R. (2014) Targeting the β secretase BACE1 for Alzheimer's disease therapy. *Lancet Neurol.* 13, 319–329.
- (6) Haass, C., and Selkoe, D. J. (2007) Soluble protein oligomers in neurodegeneration: lessons from the Alzheimer's amyloid β -peptide. *Nat. Rev. Mol. Cell Biol.* 8, 101.
- (7) Nasica-Labouze, J., Nguyen, P. H., Sterpone, F., Berthoumieu, O., Buchete, N. V., Coté, S., De Simone, A., Doig, A. J., Faller, P., Garcia, A., Laio, A., Li, M. S., Melchionna, S., Mousseau, N., Mu, Y., Paravastu, A., Pasquali, S., Rosenman, D. J., Strodel, B., Tarus, B., Viles, J. H., Zhang, T., Wang, Ch., and Derreumaux, P. (2015) Amyloid β protein and Alzheimer's disease: When computer simulations complement experimental studies. *Chem. Rev.* 115 (9), 3518–3563.
- (8) Cohen, S. I., Vendruscolo, M., Dobson, C. M., and Knowles, T. P. (2012) From macroscopic measurements to microscopic mechanisms of protein aggregation. *J. Mol. Biol.* 421, 160–171.
- (9) Lee, L. L., Ha, H., Chang, Y. T., and DeLisa, M. P. (2009) Discovery of amyloid-beta aggregation inhibitors using an engineered assay for intracellular protein folding and solubility. *Protein Sci.* 18, 277–286.
- (10) Re, F., Airoldi, C., Zona, C., Masserini, M., Ferla, B. L., Quattrocchi, N., and Nicotra, F. (2010) Beta amyloid aggregation inhibitors: small molecules as candidate drugs for therapy of Alzheimer's disease. *Curr. Med. Chem.* 17, 2990–3006.
- (11) Bednarikova, Z., Huy, P. D. Q., Mocanu, M.-M., Fedunova, D., Li, M. S., and Gazova, Z. (2016) Fullerol C 60 (OH) 16 prevents amyloid fibrillation of $\text{A}\beta$ 40–*in vitro* and *in silico* approach. *Phys. Chem. Chem. Phys.* 18, 18855–18867.
- (12) Bush, A. I. (2002) Metal complexing agents as therapies for Alzheimer's disease. *Neurobiol. Aging* 23, 1031–1038.
- (13) Neddenriep, B., Calciano, A., Conti, D., Sauve, E., Paterson, M., Bruno, E., and Moffet, D. A. (2011) Short peptides as inhibitors of amyloid aggregation. *Open Biotechnol. J.* 5, 39.
- (14) Jiang, L., Liu, C., Leibly, D., Landau, M., Zhao, M., Hughes, M. P., and Eisenberg, D. S. (2013) Structure-based discovery of fiber-binding compounds that reduce the cytotoxicity of amyloid beta. *eLife* 2, e00857.
- (15) Wang, S. H., Liu, F. F., Dong, X. Y., and Sun, Y. (2010) Thermodynamic analysis of the molecular interactions between amyloid β -peptide 42 and (–)-epigallocatechin-3-gallate. *J. Phys. Chem. B* 114 (35), 11576–11583.
- (16) Attanasio, F., Convertino, M., Magno, A., Caflisch, A., Corazza, A., Haridas, H., Esposito, G., Cataldo, D., Pignataro, B., Milardi, D., and Rizzarelli, E. (2013) Carnosine Inhibits $\text{A}\beta$ 42 Aggregation by Perturbing the H-Bond Network in and around the Central Hydrophobic Cluster. *ChemBioChem* 14 (5), 583–592.
- (17) Kroth, H., Ansaloni, A., Varisco, Y., Jan, A., Sreenivasachary, N., Rezaei-Ghaleh, N., Giriens, V., Lohmann, S., Lopez-Deber, M. P., Adolfsson, O., Pihlgren, M., Paganetti, P., Froestl, W., Nagel-Steger, L., Willbold, D., Schrader, T., Zweckstetter, M., Pfeifer, A., Lashuel, H. A., and Muhs, A. (2012) Discovery and Structure Activity Relationship of Small Molecule Inhibitors of Toxic β -amyloid-42 Fibril Formation. *J. Biol. Chem.* 287, 34786–34800.
- (18) Doig, A. J., and Derreumaux, P. (2015) Inhibition of protein aggregation and amyloid formation by small molecules. *Curr. Opin. Struct. Biol.* 30, 50–56.
- (19) Doig, A. J., del Castillo-Frias, M. P., Berthoumieu, O., Tarus, B., Nasica-Labouze, J., Sterpone, F., Nguyen, P. H., Hooper, N. M., Faller, P., and Derreumaux, P. (2017) Why Is Research on Amyloid- β Failing to Give New Drugs for Alzheimer's Disease? *ACS Chem. Neurosci.* 8, 1435–1437.
- (20) Cavalli, A., Bolognesi, M. L., Minarini, A., Rosini, M., Tumiatti, V., Recanatini, M., and Melchiorre, C. (2008) Multi-target-directed ligands to combat neurodegenerative diseases. *J. Med. Chem.* 51, 347–372.
- (21) Gazova, Z., Soukup, O., Sepsova, V., Siposova, K., Drtinova, L., Jost, P., Spilovska, K., Korabecny, J., Nepovimova, E., Fedunova, D., et al. (2017) Multi-target-directed therapeutic potential of 7-methoxytacrine-adamantylamine heterodimers in the Alzheimer's disease treatment. *Biochim. Biophys. Acta, Mol. Basis Dis.* 1863, 607–619.
- (22) Gökhane-Kelekçi, N., Koyunoğlu, S., Yabanoğlu, S., Yelekçi, K., Özgen, Ö., Uçar, G., Erol, K., Kendi, E., and Yeşilada, A. (2009) New pyrazoline bearing 4 (3H)-quinazolinone inhibitors of monoamine oxidase: Synthesis, biological evaluation, and structural determinants of MAO-A and MAO-B selectivity. *Bioorg. Med. Chem.* 17 (2), 675–689.
- (23) Mohamed, T., and Rao, P. P. (2017) 2, 4-Disubstituted quinazolines as amyloid- β aggregation inhibitors with dual cholinesterase inhibition and antioxidant properties: Development and structure-activity relationship (SAR) studies. *Eur. J. Med. Chem.* 126, 823–843.
- (24) Haghhighjoo, Z., Firuzi, O., Hemmateenejad, B., Emami, S., Edraki, N., and Miri, R. (2017) Synthesis and biological evaluation of

- quinazolinone-based hydrazones with potential use in Alzheimer's disease. *Bioorg. Chem.* 74, 126–133.
- (25) Kroth, H., Sreenivasachary, N., Hamel, A., Benderitter, P., Varisco, Y., Giriens, V., Paganetti, P., Froestl, W., Pfeifer, A., and Muhs, A. (2016) Synthesis and structure–activity relationship of 2, 6-disubstituted pyridine derivatives as inhibitors of β -amyloid-42 aggregation. *Bioorg. Med. Chem. Lett.* 26 (14), 3330–3335.
- (26) Pandolfi, F., De Vita, D., Bortolami, M., Coluccia, A., Di Santo, R., Costi, R., Andrisano, V., Alabiso, F., Bergamini, Ch., Fato, R., Bartolini, M., and Scipione, L. (2017) New pyridine derivatives as inhibitors of acetylcholinesterase and amyloid aggregation. *Eur. J. Med. Chem.* 141, 197–210.
- (27) Thai, N. Q., Nguyen, H. L., Linh, H. Q., and Li, M. S. (2017) Protocol for fast screening of multi-target drug candidates: Application to Alzheimer's disease. *J. Mol. Graphics Modell.* 77, 121–129.
- (28) Xiao, Y., Ma, B., McElheny, D., Parthasarathy, S., Long, F., Hoshi, M., Nussinov, R., and Ishii, Y. (2015) $A\beta$ (1–42) fibril structure illuminates self-recognition and replication of amyloid in Alzheimer's disease. *Nat. Struct. Mol. Biol.* 22, 499–505.
- (29) Wälti, M. A., Ravotti, F., Arai, H., Glabe, C. G., Wall, J. S., Böckmann, A., Güntert, P., Meier, B. H., and Riek, R. (2016) Atomic-resolution structure of a disease-relevant $A\beta$ (1–42) amyloid fibril. *Proc. Natl. Acad. Sci. U. S. A.* 113, E4976–E4984.
- (30) Hong, L., Turner, R. T., Koelsch, G., Shin, D., Ghosh, A. K., and Tang, J. (2002) Crystal structure of memapsin 2 (β -secretase) in complex with an inhibitor OM00–3. *Biochemistry* 41, 10963–10967.
- (31) Di Fede, G., Catania, M., Morbin, M., Rossi, G., Suardi, S., Mazzoleni, G., Merlin, M., Giovagnoli, A. R., Prioni, S., Erbetta, A., Falcone, C., Gobbi, M., Colombo, L., Bastone, A., Beeg, M., Manzoni, C., Francescucci, B., Spagnoli, A., Cantù, L., Del Favero, E., Levy, E., Salmona, M., and Tagliavini, F. (2009) A recessive mutation in the APP gene with dominant-negative effect on amyloidogenesis. *Science* 323 (5920), 1473–1477.
- (32) Nguyen, P. H., Sterpone, F., Pouplana, R., Derreumaux, P., and Campanera, J. M. (2016) Dimerization mechanism of Alzheimer $A\beta$ 40 peptides: the high content of intrapeptide-stabilized conformations in A2V and A2T heterozygous dimers retards amyloid fibril formation. *J. Phys. Chem. B* 120 (47), 12111–12126.
- (33) Murray, B., Sorci, M., Rosenthal, J., Lippens, J., Isaacson, D., Das, P., Fabris, D., Li, S., and Belfort, G. (2016) A2T and A2V $A\beta$ peptides exhibit different aggregation kinetics, primary nucleation, morphology, structure, and LTP inhibition. *Proteins: Struct., Funct., Genet.* 84 (4), 488–500.
- (34) Chen, W. T., Hong, C. J., Lin, Y. T., Chang, W. H., Huang, H. T., Liao, J. Y., Chang, Y. J., Hsieh, Y. F., Cheng, C. Y., Liu, H. C., Chen, Y. R., and Cheng, I. H. (2012) Amyloid-beta ($A\beta$) D7H mutation increases oligomeric $A\beta$ 42 and alters properties of $A\beta$ -zinc/copper assemblies. *PLoS One* 7 (4), No. e35807.
- (35) Viet, M. H., Nguyen, P. H., Derreumaux, P., and Li, M. S. (2014) Effect of the English Familial Disease Mutation (H6R) on the Monomers and Dimers of $A\beta$ 40 and $A\beta$ 42. *ACS Chem. Neurosci.* 5 (8), 646–657.
- (36) Hori, Y., Hashimoto, T., Wakutani, Y., Urakami, K., Nakashima, K., Condron, M. M., Tsubuki, S., Saido, T. C., Teplow, D. B., and Iwatsubo, T. (2007) The Tottori (D7N) and English (H6R) familial Alzheimer disease mutations accelerate $A\beta$ fibril formation without increasing protofibril formation. *J. Biol. Chem.* 282 (7), 4916–4923.
- (37) Viet, M. H., Nguyen, P. H., Ngo, S. T., Li, M. S., and Derreumaux, P. (2013) Effect of the Tottori Familial Disease Mutation (D7N) on the Monomers and Dimers of $A\beta$ 40 and $A\beta$ 42. *ACS Chem. Neurosci.* 4 (11), 1446–1457.
- (38) Yang, M., and Teplow, D. B. (2008) Amyloid β -protein monomer folding: free-energy surfaces reveal alloform-specific differences. *J. Mol. Biol.* 384 (2), 450–464.
- (39) Ngo, S. T., and Li, M. S. (2012) Curcumin binds to $A\beta$ 1–40 peptides and fibrils stronger than ibuprofen and naproxen. *J. Phys. Chem. B* 116 (34), 10165–10175.
- (40) Zhang, Y., Hashemi, M., Lv, Z., and Lyubchenko, Y. L. (2016) Self-assembly of the full-length amyloid $A\beta$ 42 protein in dimers. *Nanoscale* 8 (45), 18928–18937.
- (41) Ghosh, A. K., Brindisi, M., and Tang, J. (2012) Developing β -secretase inhibitors for treatment of Alzheimer's disease. *J. Neurochem.* 120, 71–83.
- (42) Salloway, S., Mintzer, J., Weiner, M. F., and Cummings, J. L. (2008) Disease-modifying therapies in Alzheimer's disease. *Alzheimer's Dementia* 4, 65–79.
- (43) Simone Tranches Dias, K., and Viegas, C. (2014) Multi-target directed drugs: a modern approach for design of new drugs for the treatment of Alzheimer's disease. *Curr. Neuropharmacol.* 12, 239–255.
- (44) Unzeta, M., Esteban, G., Bolea, I., Fogel, W. A., Ramsay, R. R., Youdim, M. B., Tipton, K. F., and Marco-Contelles, J. (2016) Multi-target directed Donepezil-like ligands for Alzheimer's disease. *Front. Neurosci.* 10, 205.
- (45) Martins, C., Carreiras, M. C., León, R., de los Ríos, C., Bartolini, M., Andrisano, V., Iriepa, I., Moraleda, I., Gálvez, E., García, M., et al. (2011) Synthesis and biological assessment of diversely substituted furo [2, 3-b] quinolin-4-amine and pyrrolo [2, 3-b] quinolin-4-amine derivatives, as novel tacrine analogues. *Eur. J. Med. Chem.* 46, 6119–6130.
- (46) Hamulakova, S., Poprac, P., Jomova, K., Brezova, V., Lauro, P., Drostinova, L., Jun, D., Sepsova, V., Hrabinova, M., Soukup, O., et al. (2016) Targeting copper (II)-induced oxidative stress and the acetylcholinesterase system in Alzheimer's disease using multifunctional tacrine-coumarin hybrid molecules. *J. Inorg. Biochem.* 161, 52–62.
- (47) Bischoff, F. P., Gijsen, H. J. M., Pieters, S. M. A., and Minne, G. B. (Jouve, 75001 PARIS (FR)) Substituted indazole and aza-indazole derivatives as gamma secretase modulators. European patent EP2427453 B1, 2013.
- (48) Luhrs, T., Ritter, C., Adrian, M., Riek-Lohrer, D., Bohrmann, B., Dobeli, H., Schubert, D., and Riek, R. (2005) 3D structure of Alzheimer's amyloid-beta(1–42) fibrils. *Proc. Natl. Acad. Sci. U. S. A.* 102, 17342–17347.
- (49) Tycko, R. (2016) Alzheimer's disease: Structure of aggregates revealed. *Nature* 537, 492–493.
- (50) Huy, P. D. Q., Yu, Y. C., Ngo, S. T., Thao, T. V., Chen, C. P., Li, M. S., and Chen, Y. C. (2013) In silico and in vitro characterization of anti-amyloidogenic activity of vitamin K3 analogues for Alzheimer's disease. *Biochim. Biophys. Acta, Gen. Subj.* 1830 (4), 2960–2969.
- (51) Thai, N. Q., Tseng, N. H., Vu, M. T., Nguyen, T. T., Linh, H. Q., Hu, C. K., Chen, Y. R., and Li, M. S. (2016) Discovery of DNA dyes Hoechst 34580 and 33342 as good candidates for inhibiting amyloid beta formation: in silico and in vitro study. *J. Comput.-Aided Mol. Des.* 30 (8), 639–650.
- (52) Huy, P. D. Q., Vuong, Q. V., La Penna, G., Faller, P., and Li, M. S. (2016) Impact of Cu (II) binding on structures and dynamics of $A\beta$ 42 monomer and dimer: Molecular dynamics study. *ACS Chem. Neurosci.* 7 (10), 1348–1363.
- (53) Man, V. H., Nguyen, P. H., and Derreumaux, P. (2017) High-resolution structures of the amyloid- β 1–42 dimers from the comparison of four atomistic force fields. *J. Phys. Chem. B* 121 (24), 5977–5987.
- (54) Lindorff-Larsen, K., Piana, S., Palmo, K., Maragakis, P., Klepeis, J. L., Dror, R. O., and Shaw, D. E. (2010) Improved side-chain torsion potentials for the Amber ff99SB protein force field. *Proteins: Struct., Funct., Genet.* 78, 1950–1958.
- (55) Carballo-Pacheco, M., and Strodel, B. (2017) Comparison of force fields for Alzheimer's A β 42: A case study for intrinsically disordered proteins. *Protein Sci.* 26 (2), 174–185.
- (56) Jorgensen, W. L., Chandrasekhar, J., Madura, J. D., Impey, R. W., and Klein, M. L. (1983) Comparison of simple potential functions for simulating liquid water. *J. Chem. Phys.* 79, 926–935.
- (57) Wang, J., Wang, W., Kollman, P. A., and Case, D. A. (2001) Antechamber: an accessory software package for molecular mechanical calculations. *Abs. Pap. Am. Chem. Soc.* 222, U403.

- (58) Sousa da Silva, A. W., and Vranken, W. F. (2012) ACPYPE-Antechamber p ython parser interface. *BMC Res. Notes* 5, 367.
- (59) Wang, J., Wolf, R. M., Caldwell, J. W., Kollman, P. A., and Case, D. A. (2004) Development and testing of a general amber force field. *J. Comput. Chem.* 25, 1157–1174.
- (60) Jakalian, A., Bush, B. L., Jack, D. B., and Bayly, C. I. (2000) Fast, efficient generation of high-quality atomic Charges. AM1-BCC model: I. Method. *J. Comput. Chem.* 21, 132–146.
- (61) Darden, T., York, D., and Pedersen, L. (1993) Particle mesh Ewald: An N· log (N) method for Ewald sums in large systems. *J. Chem. Phys.* 98, 10089–10092.
- (62) Hockney, R., Goel, S., and Eastwood, J. (1974) Quiet high-resolution computer models of a plasma. *J. Comput. Phys.* 14, 148–158.
- (63) Bartholomew-Biggs, M. (2005) The steepest descent method. *Nonlinear Optimization with Financial Applications*, 51–64.
- (64) Berendsen, H. J., Postma, J. V., van Gunsteren, W. F., DiNola, A. R. H. J., and Haak, J. R. (1984) Molecular dynamics with coupling to an external bath. *J. Chem. Phys.* 81 (8), 3684–3690.
- (65) Parrinello, M., and Rahman, A. (1981) Polymorphic transitions in single crystals: A new molecular dynamics method. *J. Appl. Phys.* 52, 7182–7190.
- (66) Kollman, P. A., Massova, I., Reyes, C., Kuhn, B., Huo, S., Chong, L., Lee, M., Lee, T., Duan, Y., Wang, W., et al. (2000) Calculating structures and free energies of complex molecules: combining molecular mechanics and continuum models. *Acc. Chem. Res.* 33, 889–897.
- (67) Nguyen, T. T., Mai, B. K., and Li, M. S. (2011) Study of Tamiflu sensitivity to variants of A/H5N1 virus using different force fields. *J. Chem. Inf. Model.* 51, 2266–2276.
- (68) Duan, L., Liu, X., and Zhang, J. Z. H. (2016) Interaction Entropy: A New Paradigm for Highly Efficient and Reliable Computation of Protein–Ligand Binding Free Energy. *J. Am. Chem. Soc.* 138, 5722–5728.

SUPPORTING INFORMATION

CID 9998128 compound is a potential multi-target drug for Alzheimer's disease

Nguyen Quoc Thai^{1,2,3,†}, Zuzana Bednarikova^{4†}, Miroslav Gancar⁴, Huynh Quang Linh³, Chin-Kun Hu^{5,6,7,8*}, Mai Suan Li^{9*}, and Zuzana Gazova^{4*}

¹*Institute for Computational Sciences and Technology, SBI building, Quang Trung Software city, Tan Chanh Hiep Ward, District 12, Ho Chi Minh City, Vietnam*

²*Dong Thap University, 783 Pham Huu Lau Street, Ward 6, Cao Lanh City, Dong Thap, Vietnam*

³*Biomedical Engineering Department, University of Technology -VNU HCM, 268 Ly Thuong Kiet Str., Distr. 10, Ho Chi Minh City, Vietnam*

⁴*Department of Biophysics, Institute of Experimental Physics, Slovak Academy of Sciences, Watsonova 47, Kosice, Slovakia*

⁵*Institute of Physics, Academia Sinica, Nankang, Taipei 11529, Taiwan*

⁶*Physics Division, National Center for Theretical Sciences, Hsinchu 30013, Taiwan*

⁷*Department of Physics, National Dong Hwa University, Hualien 97401, Taiwan*

⁸*Department of Systems Science, University of Schanghai for Science and Technology, Shanghai 200093, China*

⁹*Institute of Physics, Polish Academy of Sciences, Al. Lotnikow 32/46, 02-668 Warsaw, Poland*

†These authors contributed equally

*Email: gazova@saske.sk, masli@ifpan.edu.pl, huck@phys.sinica.edu.tw

Binding free energy of CID 9998128 to A β fibrils and β -secretase

Table S1. Binding free energy ΔG_{bind} (kcal/mol) to truncated A β_{11-42} (2MXU) fibril. Results were obtained by the MM-PBSA method in four MD trajectories.

Q128	ΔE_{ele}	ΔE_{vdw}	ΔG_{PB}	ΔG_{sur}	$-T\Delta S$	ΔG_{bind} (kcal/mol)
1	-6.9	-44.7	26.3	-6.1	8.5	-22.9
2	-7.4	-41.8	23.6	-5.9	8.4	-23.1
3	-6.7	-46.7	29.9	-6.4	8.1	-21.8
4	-8.8	-39.7	26.7	-5.7	5.8	-21.7
Average	-7.4 ± 0.8	-43.2 ± 2.7	26.6 ± 2.2	-6.0 ± 0.3	7.7 ± 1.1	-22.4 ± 0.6

Table S2. Binding free energy ΔG_{bind} (kcal/mol) to full length A β_{1-42} (2NAO) fibril. Results were obtained by the MM-PBSA method in four MD trajectories.

Q128	ΔE_{ele}	ΔE_{vdw}	ΔG_{PB}	ΔG_{sur}	$-T\Delta S$	ΔG_{bind} (kcal/mol)
1	-9.4	-45.4	26.2	-6.0	10.5	-24.0
2	-9.4	-35.5	18.0	-6.0	7.8	-25.1
3	-7.2	-32.6	15.5	-4.4	8.5	-20.2
4	-10.6	-42.0	26.8	-5.3	6.9	-24.2
Average	-9.1 ± 1.2	-38.9 ± 5.0	21.6 ± 4.9	-5.4 ± 0.6	8.4 ± 1.3	-23.4 ± 1.8

Table S3. Binding free energy ΔG_{bind} (kcal/mol) to β -secretase (1M4H). Results were obtained by the MM-PBSA method in four MD trajectories.

Q128	ΔE_{ele}	ΔE_{vdw}	ΔG_{PB}	ΔG_{sur}	$-T\Delta S$	ΔG_{bind} (kcal/mol)
1	-19.7	-32.9	32.1	-5.6	6.8	-19.3
2	-17.5	-34.4	31.3	-5.6	6.1	-20.1
3	-16.9	-32.4	30.5	-5.5	5.6	-18.7
4	-16.6	-31.7	30.0	-5.6	6.9	-17.0
Average	-17.7 ± 1.2	-32.8 ± 1.0	31.0 ± 0.8	-5.6 ± 0.1	6.3 ± 0.5	-18.8 ± 1.1

Table S4. Name, charge and mass of ligand atoms that belong to different blocks. Nr refers to atom number shown in Fig. 1 in the main text.

Block	Nr	Type	Atom	Charge	Mass
Block 1	1	nb	N	-0.741	14.010
	2	nb	N1	-0.705	14.010
	3	ca	C	-0.288	12.010
	4	ca	C1	0.693	12.010
	5	ca	C2	0.438	12.010
	6	cp	C3	0.637	12.010
	7	ca	C4	-0.094	12.010
	8	ca	C5	-0.177	12.010
	9	ca	C6	-0.141	12.010
	10	ca	C7	-0.105	12.010
	30	ha	H2	0.130	1.008
	31	ha	H3	0.157	1.008
	32	ha	H4	0.137	1.008
	33	ha	H5	0.138	1.008
Total charge				0.079	
Block 2	11	nh	N2	-0.717	14.010
	12	hn	H	0.425	1.008
	13	ca	C8	0.092	12.010
	14	ca	C9	-0.034	12.010
	15	ca	C10	-0.202	12.010
	16	ca	C11	-0.064	12.010
	17	cc	C12	0.355	12.010
	18	na	N3	-0.019	14.010
	19	ca	C13	-0.126	12.010
	20	nd	N4	-0.514	14.010
	21	hn	H1	0.315	1.008
	22	ca	C14	-0.131	12.010
	34	ha	H6	0.168	1.008
	35	h4	H7	0.058	1.008
	36	ha	H8	0.140	1.008
	37	ha	H9	0.130	1.008
Total charge				-0.124	
Block 3	23	cp	C15	0.377	12.010
	24	nb	N5	-0.64	12.010
	25	ca	C16	0.412	14.010
	26	ca	C17	-0.241	12.010
	27	c3	C18	-0.148	12.010
	28	ca	C19	-0.095	12.010
	29	ca	C20	-0.216	12.010
	38	ha	H10	0.143	1.008
	39	hc	H11	0.042	1.008
	40	hc	H12	0.058	1.008
	41	hc	H13	0.06	1.008
	42	ha	H14	0.139	1.008
	43	ha	H15	0.154	1.008
Total charge				0.045	

Table S5. Contributions of three blocks to the interaction with targets. Results were obtained using MD simulation.

Q128	Block 1		Block 2		Block 3	
	ΔE_{ele}	ΔE_{vdw}	ΔE_{ele}	ΔE_{vdw}	ΔE_{ele}	ΔE_{vdw}
2MXU	-5.8 ± 1.5	-15.1 ± 0.9	0.8 ± 1.4	-15.2 ± 2.2	-2.6 ± 1.0	-14.1 ± 0.2
2NAO	-25.8 ± 1.8	-15.2 ± 2.5	25.4 ± 3.7	-15.5 ± 1.5	-9.7 ± 1.1	-7.9 ± 3.1
1M4H	-5.6 ± 0.5	-11.0 ± 0.4	4.0 ± 0.9	-10.2 ± 0.2	-15.7 ± 0.6	-12.1 ± 0.4

Table S6. Residues forming HB and non-bonded contact with CID 9998128. Results were obtained for 2MXU, 2NAO, and 1M4H using MD simulation.

Target	Mean HBs	Mean NBCs	Residues form HB with CID 9998128	Residues form NBC with CID 9998128
2MXU	0.5	21.9	Glu11(A), Glu11(D), His14(A), His14(B), Ile32(E), Gly33(D), Leu34(E)	Glu11(A), Glu11(D), Glu11(B), Val12(A), Val12(B), Val12(C), Val12(D), Hie13(A), Hie13(B), Hie14(A), Hie14(B), Hie14(C), Hie14(D), Hie14(E), Lys16(A), Leu17(A), Leu17(B), Leu17(C), Leu17(D), Leu17(E), Leu17(F), Val18(D), Val18(E), Phe19(D), Phe19(C), Phe19(E), Phe19(B), Phe19(A), Phe19(F), Ala30(A), Ala30(B), Ile32(A), Ile32(B), Ile32(C), Ile32(D), Ile32(E), Ile32(F), Gly33(A), Gly33(B), Gly33(C), Gly33(D), Gly33(E), Gly33(F), Leu34(B), Leu34(C), Leu34(D), Leu34(A), Leu34(E), Leu34(F), Met35(B), Met35(C), Val36(D)
2NAO	1.4	14.1	His6(F), Ser8(E), Gly9(E), Tyr10(D), Glu11(D), Val12(E), His13(E), His14(E), Gln15(D), Lys16(D), Gly38(B)	Asp1(F), Ala2(F), Ala2(E), Glu3(F), Glu3(E), Phe4(D), Phe4(E), Phe4(F), Arg5(F), His6(D), His6(E), His6(F), Asp7(E), Asp7(D), Ser8(E), Ser8(F), Ser8(D), Gly9(E), Gly9(F), Gly9(D), Tyr10(D), Tyr10(E), Tyr10(F), Glu11(E), Glu11(D), Glu11(F), Val12(D), Val12(E), Val12(F), His13(E), His13(D), His13(F), His14(D), His14(E), His14(F), Gln15(D), Gln15(E), Gln15(F), Lys16(D), Lys16(E), Val36(C), Gly37(B), Gly37(A), Gly37(C), Gly38(B), Gly38(A), Gly38(C), Val39(A), Val39(B), Val39(C), Val40(A), Val40(B), Val40(C), Ile41(A), Ile41(B), Ala42(A), Ala42(B)
1M4H	1.6	20.6	Thr72(A), Gln73(A), Arg128(A), Tyr198(A), Lys224(A), Asp228(A), Thr231(A), Arg235(A), Ser327(A), Ser328(A), Thr329(A)	Leu30(A), Asp32(A), Gly34(A), Ser35(A), Val69(A), Pro70(A), Tyr71(A), Thr72(A), Gln73(A), Gly74(A), Phe108(A), Ile110(A), Trp115(A), Ile118(A), Ile126(A), Tyr198(A), Lys224(A), Ile226(A), Asp228(A), Gly230(A), Thr231(A), Arg235(A), Ser325(A), Ser327(A), Thr329(A), Val332(A), Thr33(A), Ala122(A), Asn233(A), Gly330(A), Ser113(A), Thr232(A), Gly11(A), Ser328(A), Gly13(A), Ser229(A), Phe109(A), Gln12(A), Lys107(A), Gln326(A), Arg128(A), Gly117(A), Asp223(A)

Table S7. Binding free energy of CID 9998128 to A β ₁₋₄₂ monomer. The results were obtained by MMPB-SA method for 9 models. The interaction energies are measured in kcal/mol.

CID 9998128 models	ΔE_{ele}	ΔE_{vdW}	ΔE_{PB}	ΔE_{SA}	$-T\Delta S$	ΔG_{bind}
1	-8.6	-36.9	18.9	-4.9	6.9	-24.4 ± 6.1
2	-20.9	-33.1	27.0	-4.9	8.6	-23.1 ± 4.6
3	-17.7	-29.7	18.3	-4.1	7.9	-25.2 ± 1.8
4	-10.4	-33.6	16.0	-4.7	7.8	-24.9 ± 3.8
5	-14.8	-36.4	20.6	-5.1	8.3	-27.3 ± 3.9
6	-13.1	-32.4	17.4	-4.6	7.1	-25.6 ± 2.2
7	-11.7	-38.5	21.8	-5.0	8.7	-24.8 ± 4.3
8	-16.3	-30.9	22.8	-4.0	7.5	-20.8 ± 5.9
9	-14.6	-34.4	18.5	-4.8	8.1	-27.2 ± 1.9
Average	-14.2	-34.0	20.1	-4.6	7.9	-24.8 ± 1.8

Table S8. Binding free energy of CID 9998128 to A β ₁₋₄₂ dimer in 4 MD trajectories. The results were obtained by MMPB-SA method. The unit of interaction energies is kcal/mol.

A β ₁₋₄₂ dimer /Traj	ΔE_{ele}	ΔE_{vdW}	ΔE_{PB}	ΔE_{SA}	$-T\Delta S$	ΔG_{bind}
1	-20.3	-20.9	20.1	-2.9	4.9	-19.1
2	-9.7	-30.5	16.4	-4.3	4.0	-24.1
3	-12.3	-22.4	13.6	-3.4	5.7	-18.8
4	-12.7	-32.7	17.9	-4.7	6.8	-25.4
Average	-13.7 ± 3.9	-26.6 ± 5.0	17.0 ± 2.3	-3.8 ± 0.6	5.3 ± 1.0	-21.8 ± 2.9



Figure S1. The fibril A β 1-42 structure (2NAO) with five best docking modes of CID 9998128. The first amino acids are highlighted by small balls.

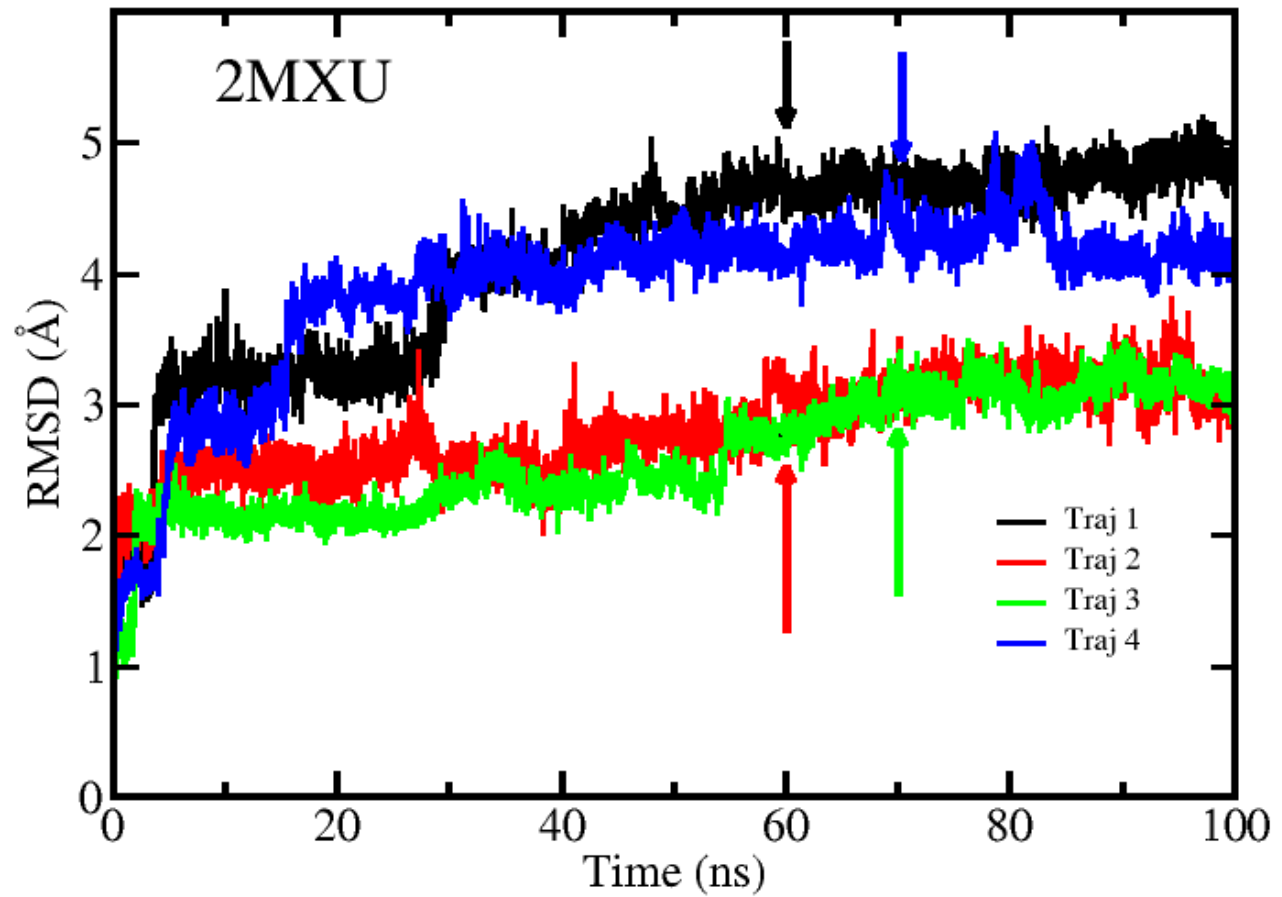


Figure S2. Time dependence of RMSD of target $\text{A}\beta_{11-42}$ (2MXU)+ CID 9998128 complex. The arrow refers to time when the system reaches equilibrium.

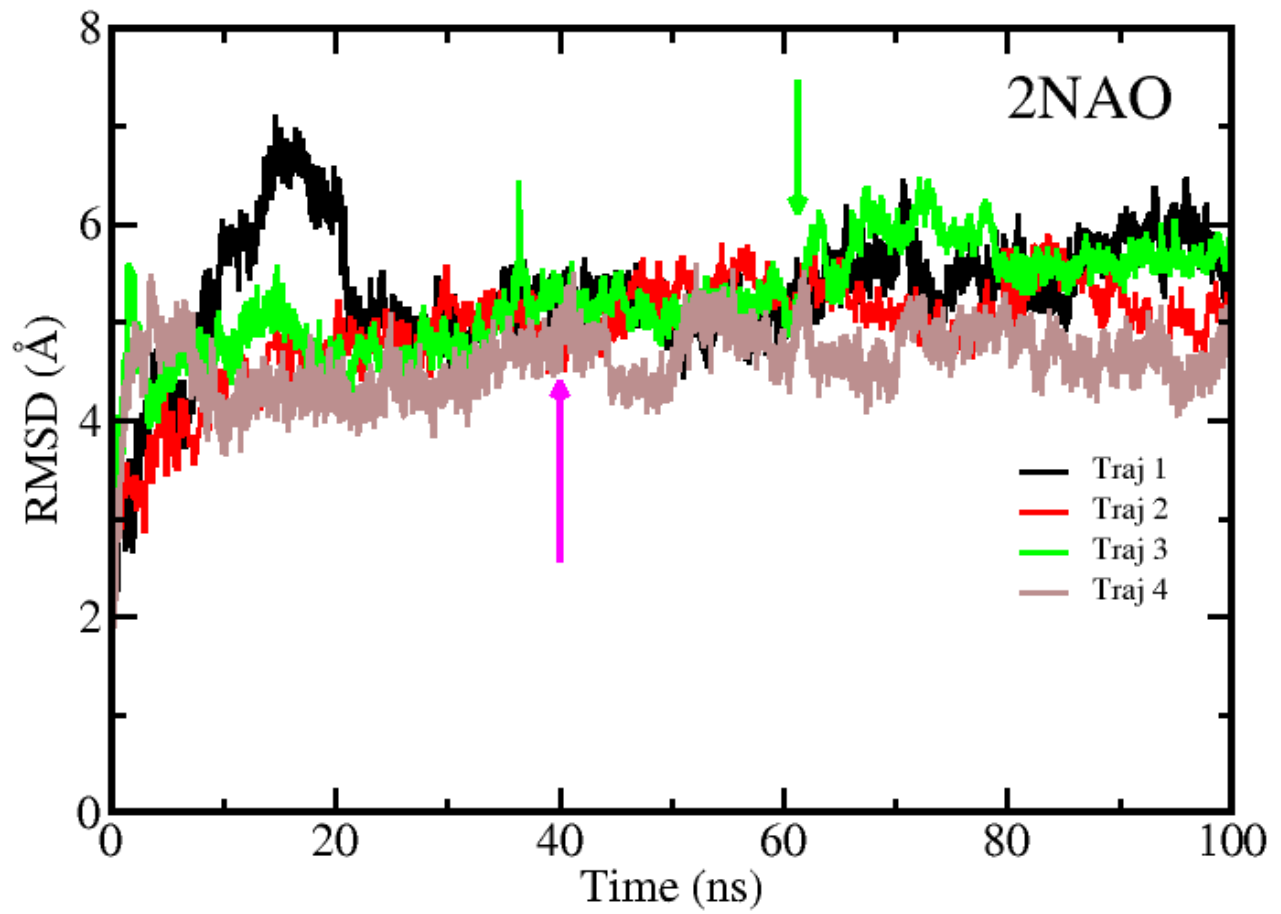


Figure S3. Time dependence of RMSD of target A β ₁₋₄₂ (2NAO)+ CID 9998128 complex. The magenta arrow refers to time when the system reaches equilibrium in trajectories 1, 2 and 4 (40 ns), while the green arrow – trajectory 3 (60 ns).

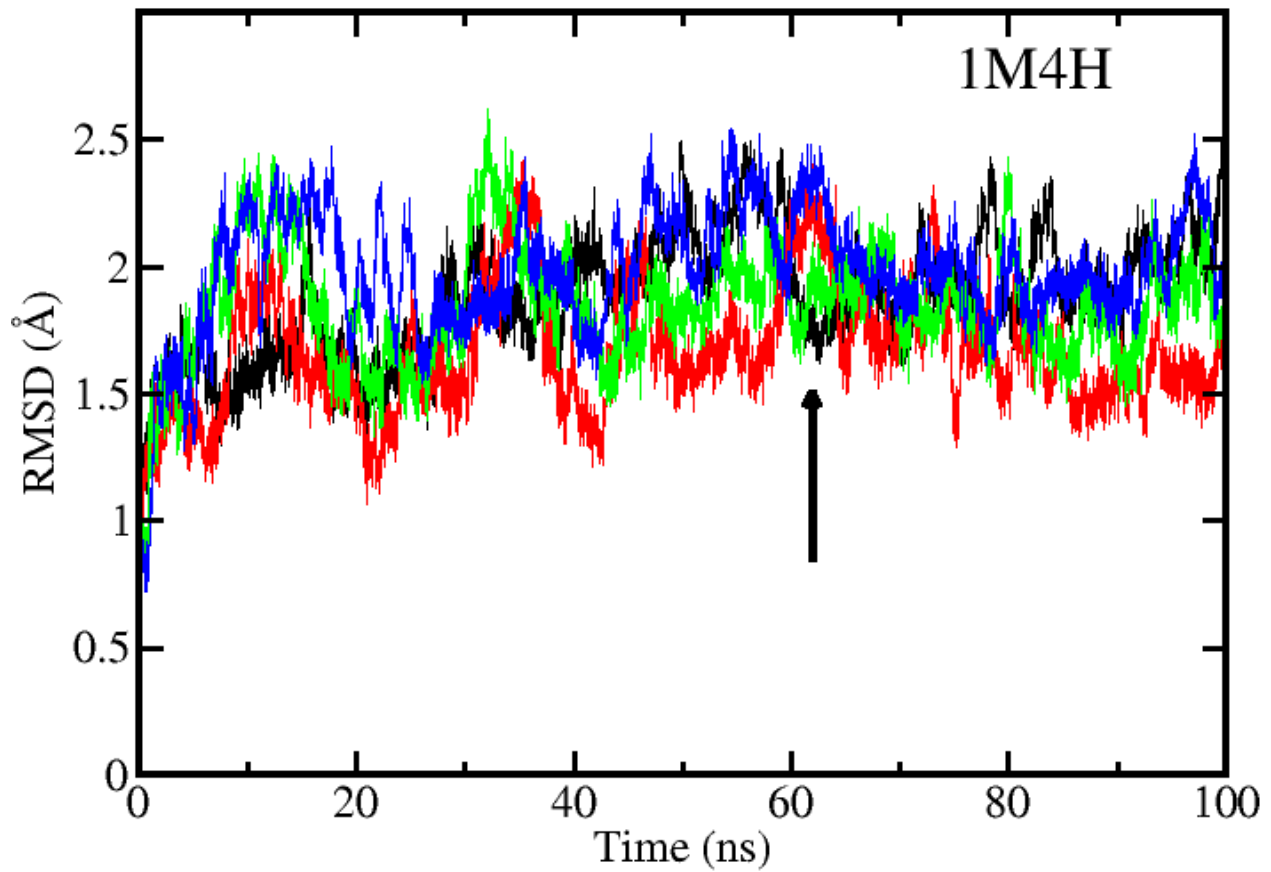


Figure S4. Time dependence of RMSD of target β -secretase (1M4H)+ [CID 9998128](#) complex. The arrow refers to time when the system reaches equilibrium in all MD runs (60 ns).

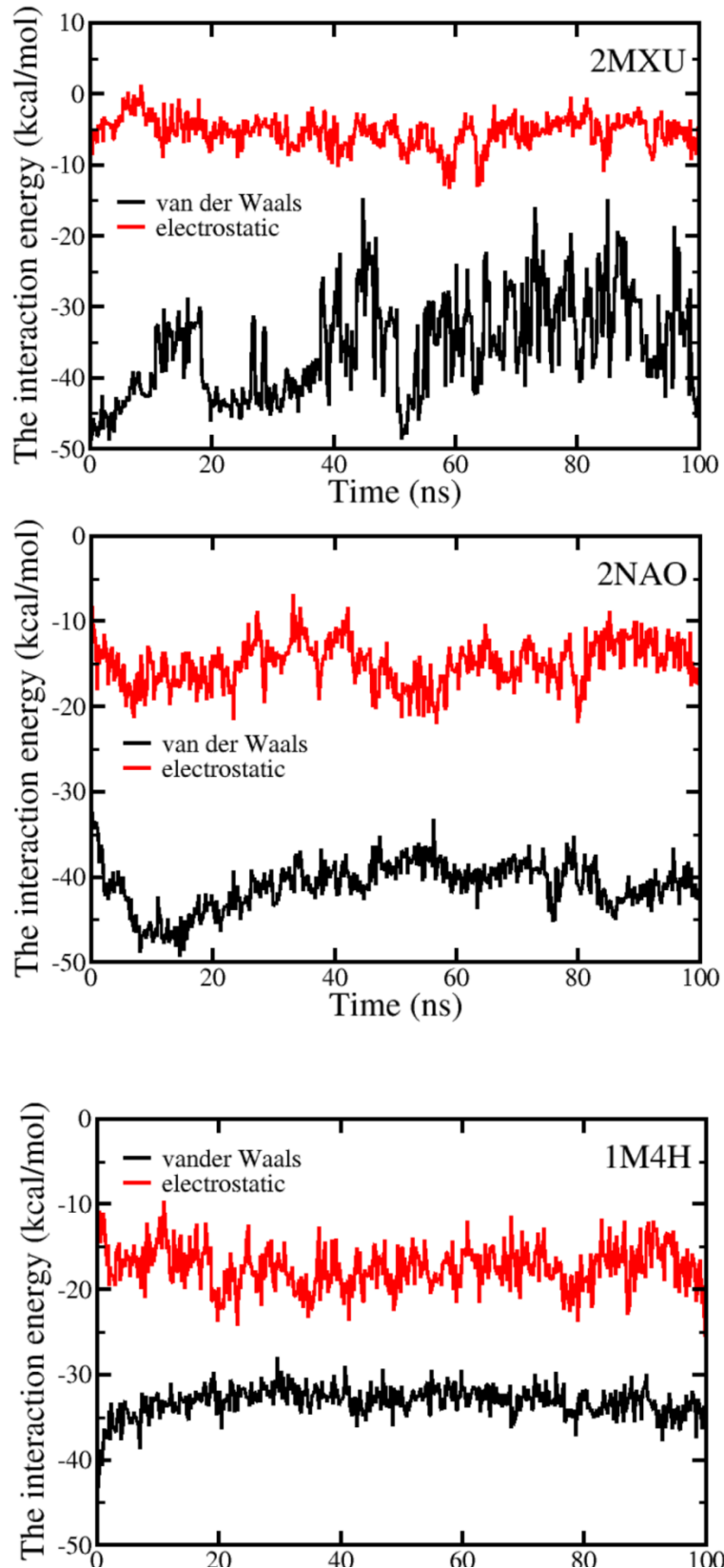


Figure S5. Time dependence of the electrostatics and van der Waals interaction energies between CID 9998128 and three targets.

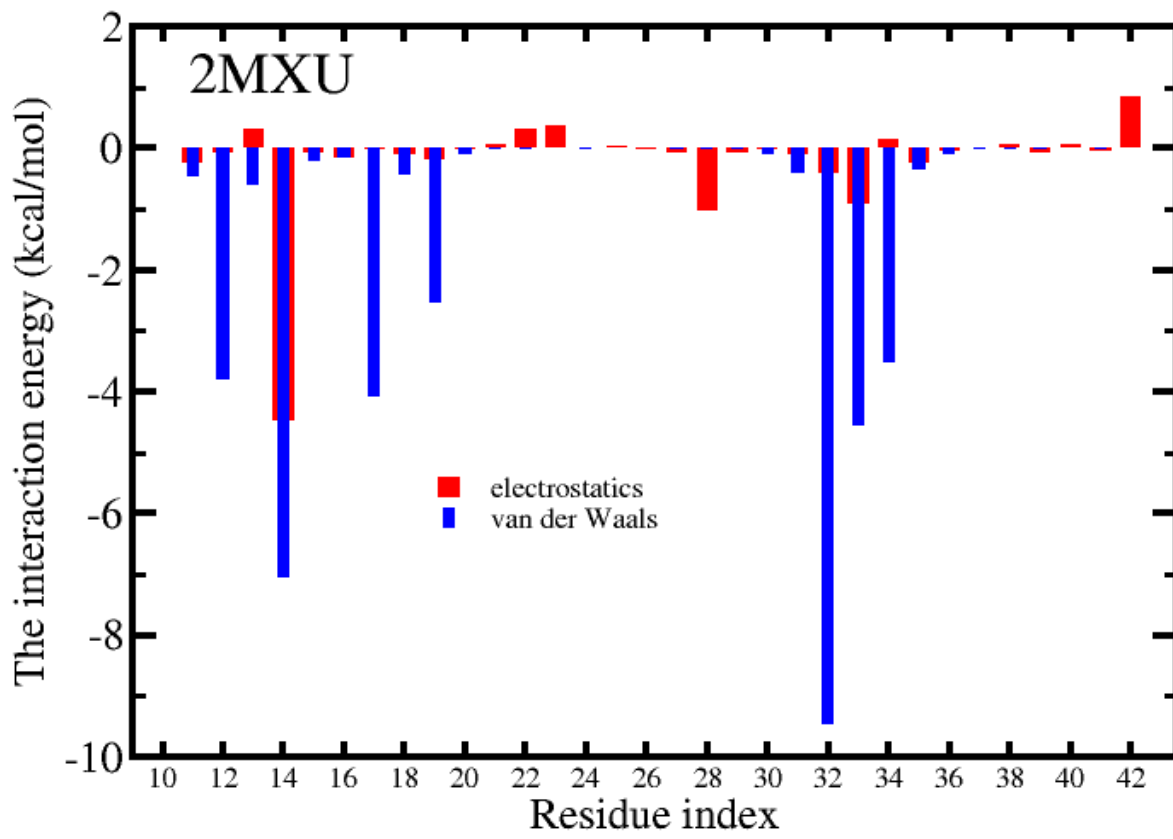


Figure S6. Per-residue distributions of the electrostatic and vdW interactions of A β ₁₁₋₄₂ fibril (2MXU) with CID 9998128. The results were obtained at equilibrium and averaged over chains in 4 MD trajectories.

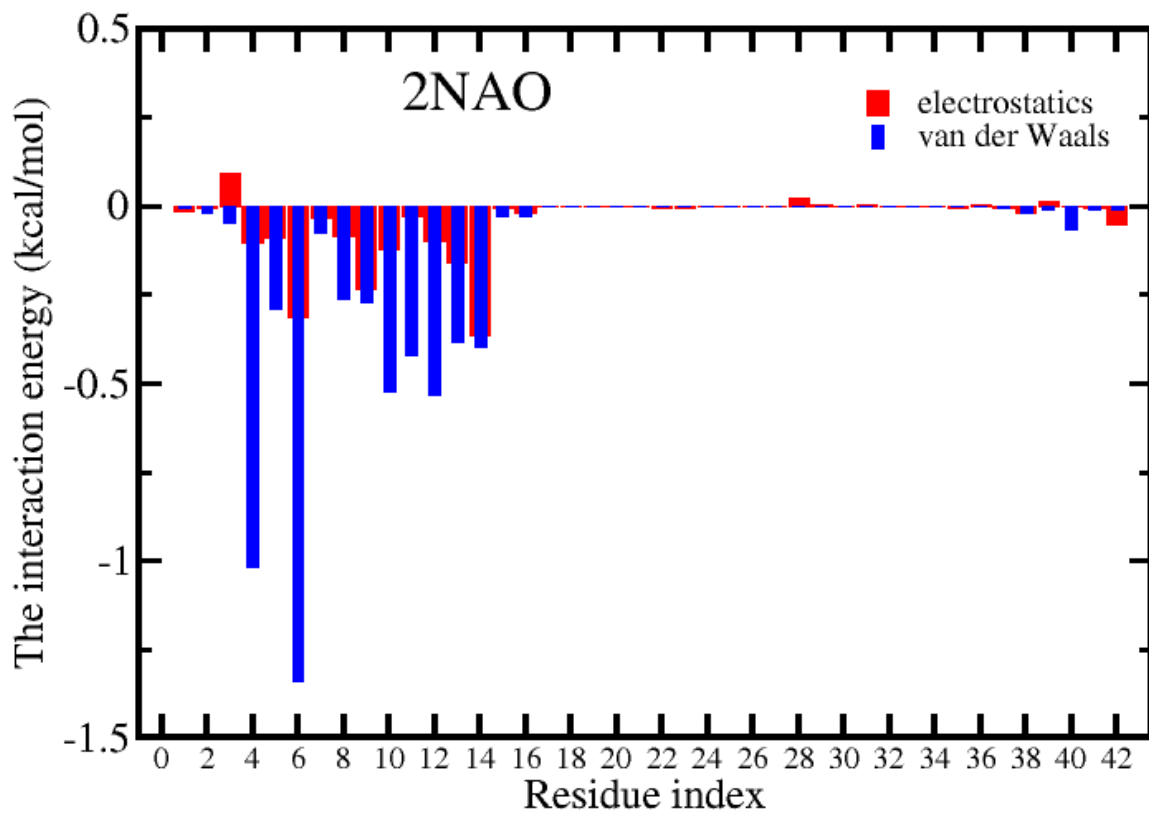


Figure S7. Per-residue distributions of the electrostatic and vdW interactions of $\text{A}\beta_{1-42}$ fibril (2NAO) with CID 9998128. The results were obtained at equilibrium and averaged over chains in 4 MD trajectories.

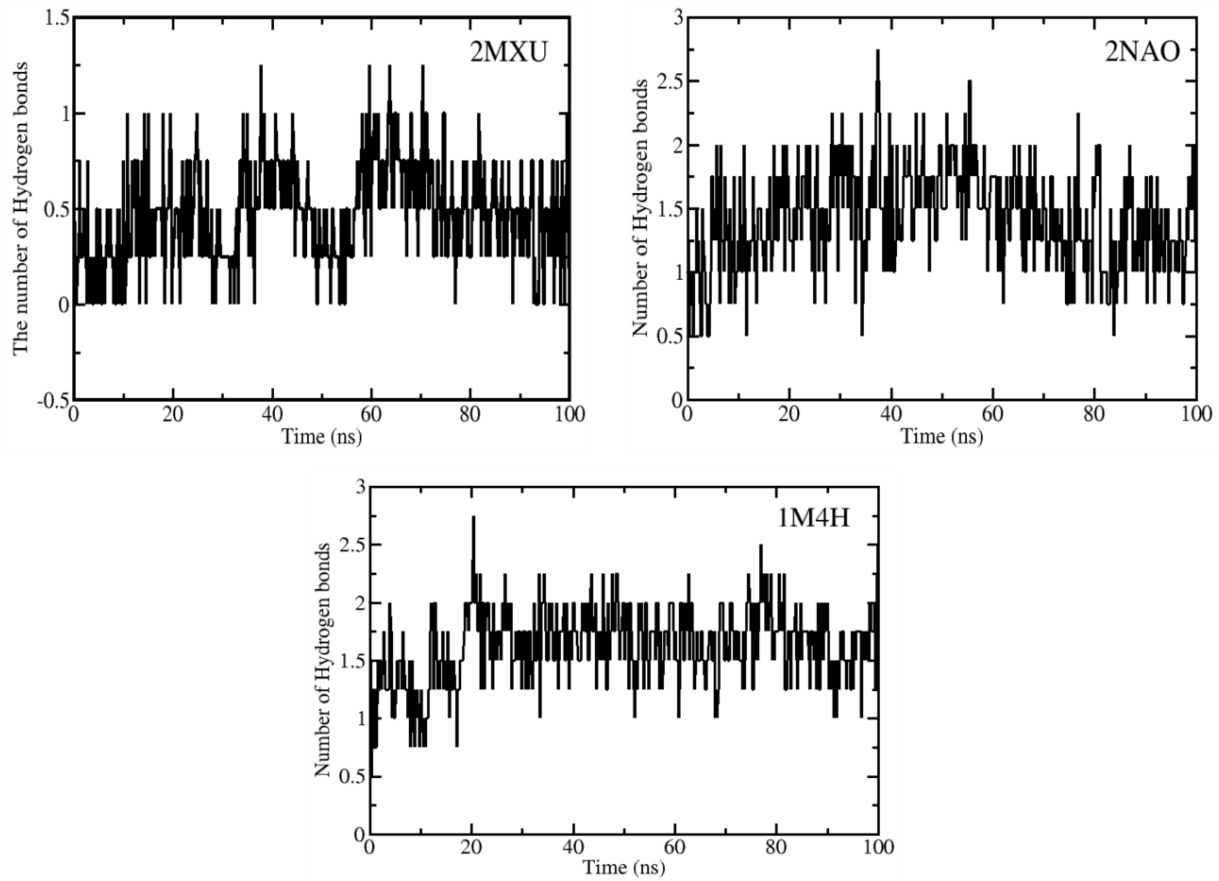


Figure S8. Time dependence of the number of HBs formed by CID 9998128 with target during MD simulation.

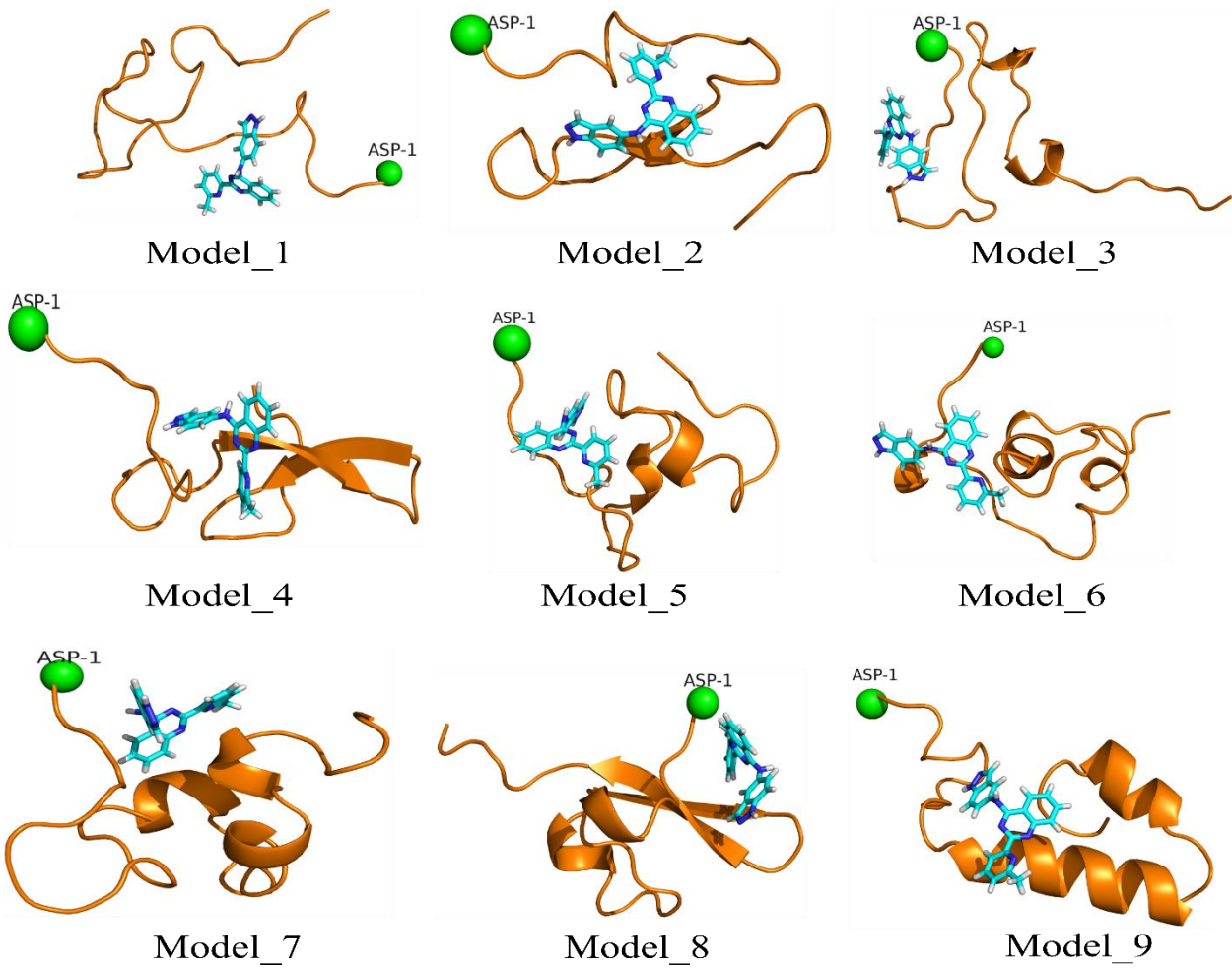


Figure S9. Nine models of A β 1-42 monomer, obtained by MD simulation, in the best docking mode with CID 9998128. The green sphere refers to the first amino acid of A β ₁₋₄₂.

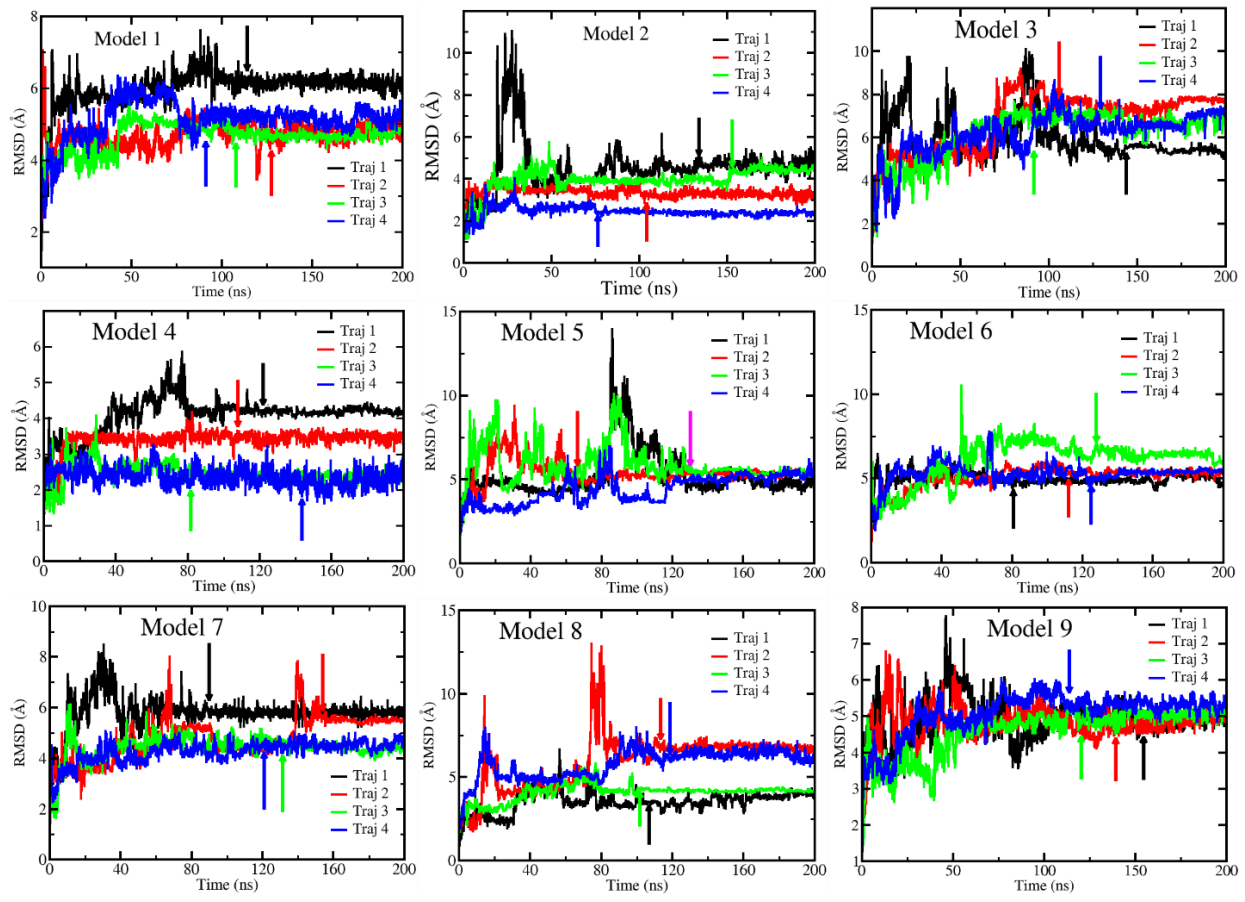


Figure S10. The time dependence of RMSD of A β 1-42 monomer with CID 9998128. The arrow indicates time when the complex reaches equilibrium.

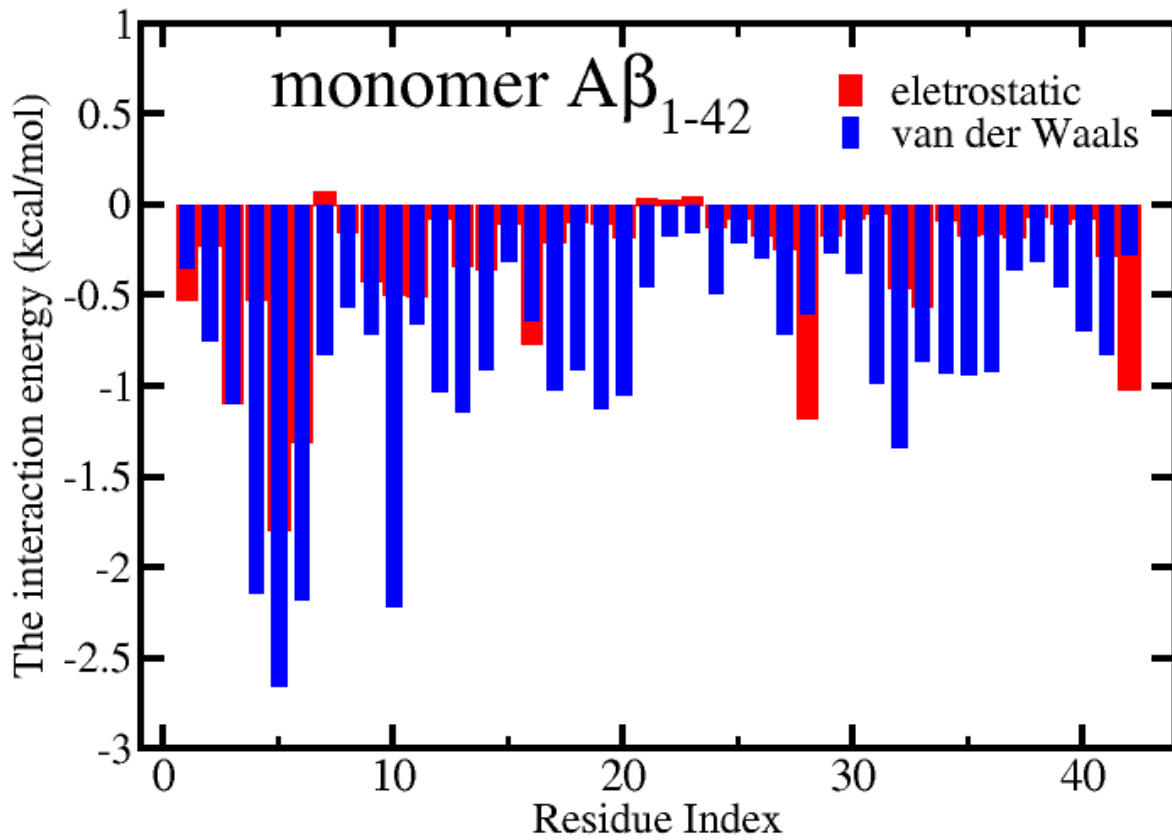


Figure S11. Per-residue distributions of the electrostatic and vdW interactions of A β ₁₋₄₂ monomer with CID 9998128. The results were obtained at equilibrium and averaged over 9 model for each model with 4 trajectories.

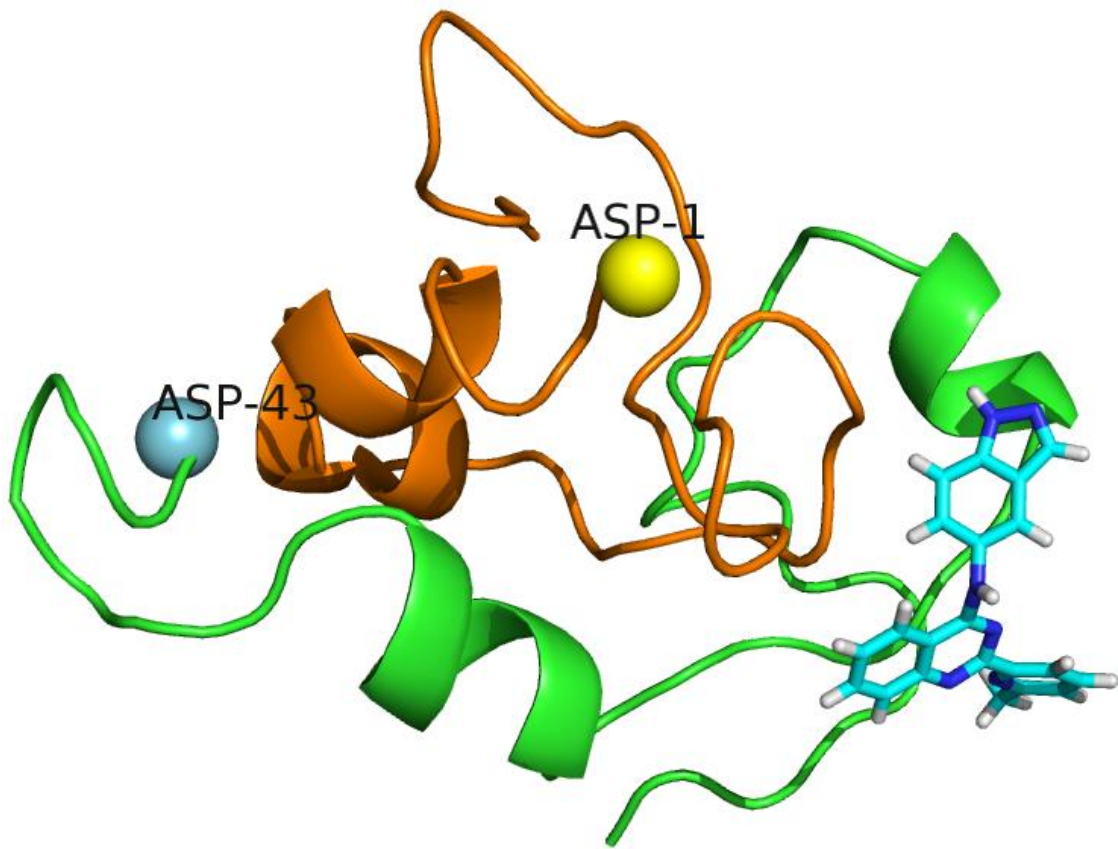


Figure S12. The best docking model of A β 1-42 dimer with CID 9998128. Chain A is showed orange, chain B is showed green, while the sphere refers to the first amino acid of chain.

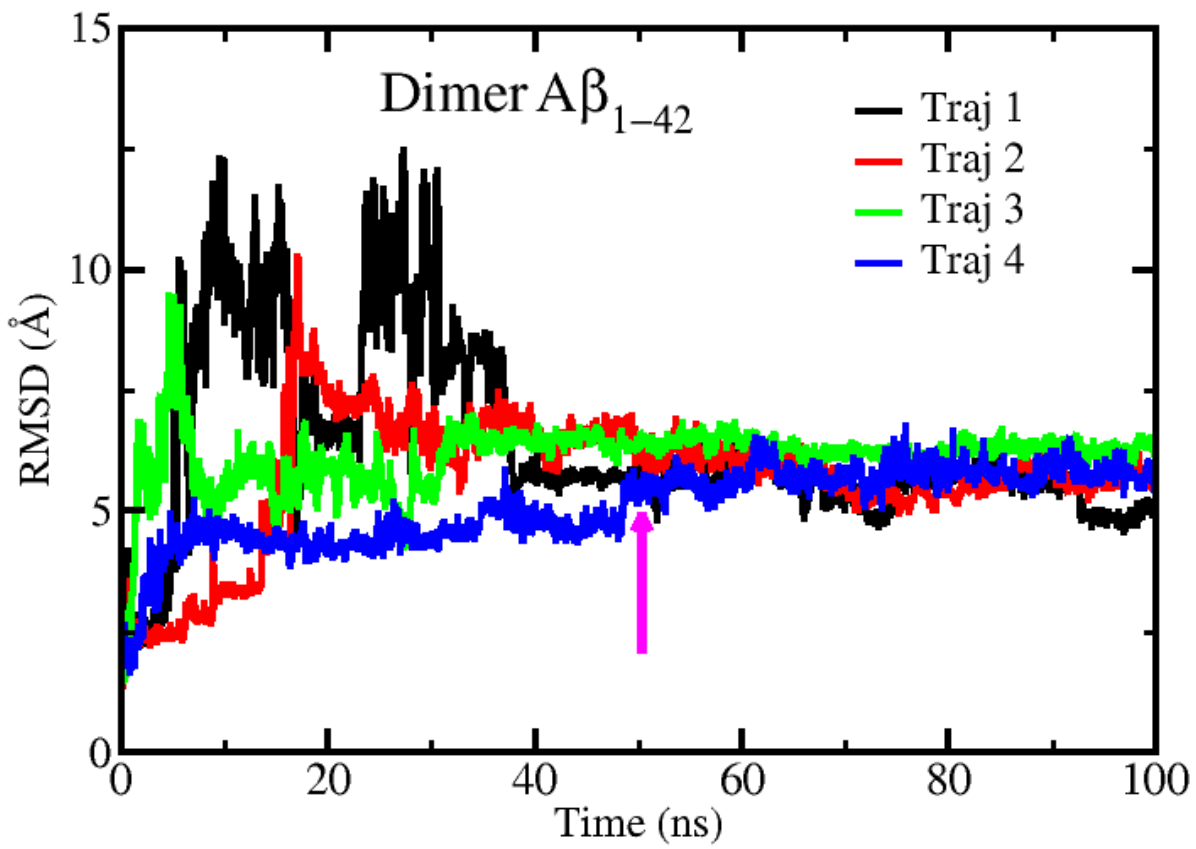


Figure S13. The time dependence of RMSD of A β 1-42 dimer in complex with CID 9998128. The magenta arrow shows time (50ns) when the complex reaches equilibrium in all of 4 trajectories.

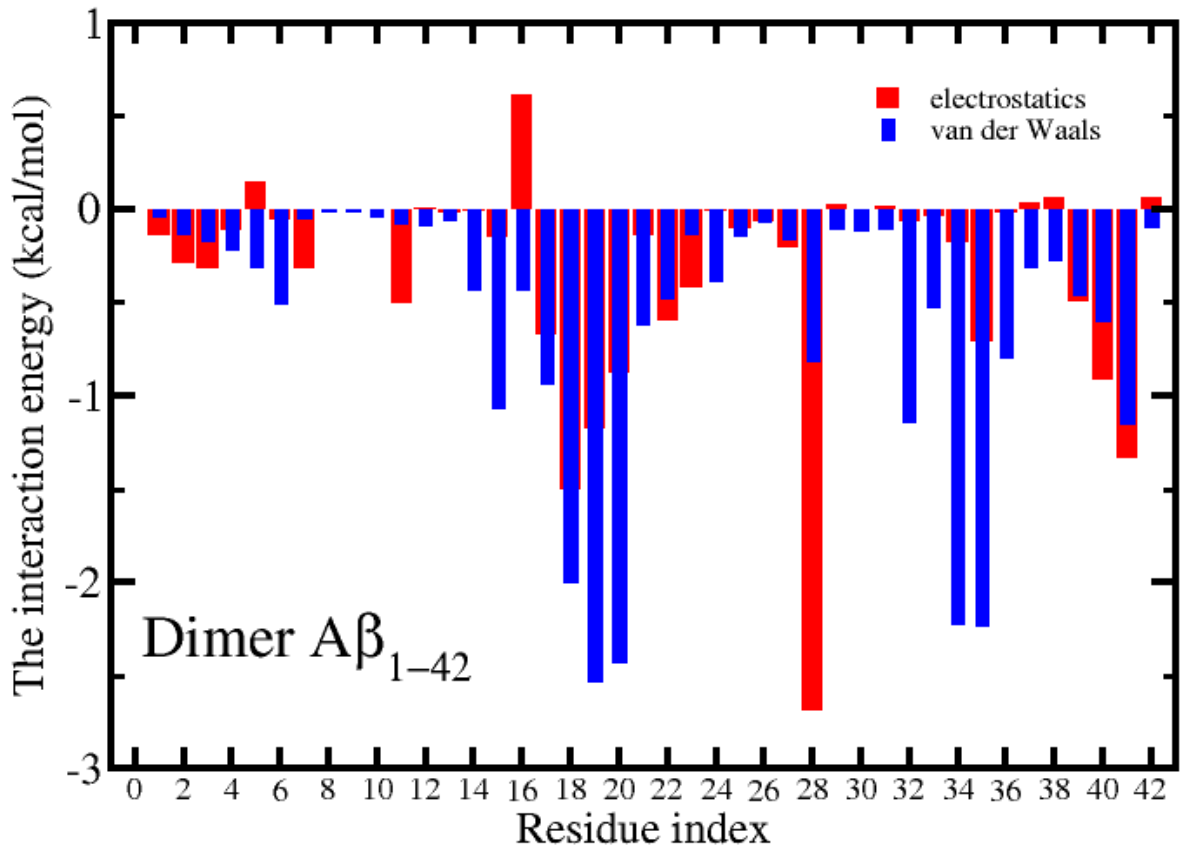


Figure S14. Per-residue distributions of the electrostatic and vdW interactions of A β ₁₋₄₂ dimer with CID 9998128. The results were obtained at equilibrium and averaged over 4 trajectories.

MOVIES

Movie 1. Movement of CID 9998128 in the binding site of β -secretase at equilibrium.

Movie 2. Movement of CID 9998128 around full-length 2NAO fibril during MD simulation.